MODIFIED BOUSSINESQ EQUATIONS AND ASSOCIATED PARABOLIC MODELS FOR WAVE PROPAGATION

by

YONGZE CHEN and PHILIP L.-F. LIU

RESEARCH REPORT NO. CACR-93-06

July, 1993

CENTER FOR APPLIED COASTAL RESEARCH

Department of Civil Engineering
University of Delaware
Newark, Delaware 19716

Modified Boussinesq equations and associated parabolic models for wave propagation

Yongze Chen and Philip L.-F. Liu
School of Civil and Environmental Engineering
Cornell University, Ithaca, NY 14853, U.S.A.

Abstract

Modified Boussinesq equations are derived in terms of the velocity potential on an arbitrary elevation and the free surface displacement. Phase velocity and group velocity associated with the linearized modified Boussinesq equations are compared with those given by the Stokes first-order theory over a wide range of water depths. To determine the optimal elevation where the velocity potential should be evaluated, the summation of relative errors of phase and group velocities over a range of depths from zero to half of the equivalent deep water depth is minimized. For regular waves propagating over a mild-slope topography, a small-angle parabolic approximation model is developed and solved by the pseudospectral Chebyshev method. The pseudospectral Fourier method used by Chen & Liu (1993) is employed to derive a wide-angle parabolic approximation model for multi-directional wave propagation. The small-angle model is examined by comparing numerical results with the experimental data of Whalin (1971). The wide-angle model is tested by comparing numerical results with the refraction theory of cnoidal waves (Skovgaard & Petersen, 1977) and is used to study the impact of the directed wave angle on the oblique interaction of two identical cnoidal wavetrains in shallow water.

1 Introduction

Boussinesq-type equations, which are conventionally expressed in terms of the depth-averaged horizontal velocity (Peregrine, 1967), have been commonly used to describe weakly nonlinear and dispersive wave propagation in shallow water. They are capable of modelling the combined effects of shoaling, refraction, reflection and diffraction of finite amplitude, irregular waves propagating over a complex topography. These equations are derived based on the assumption that the weakly nonlinearity represented by the ratio of wave amplitude to water depth, $\varepsilon = a_0/h_0$, is in the same order of magnitude as the frequency dispersion denoted by the square of the ratio of water depth to wavelength, $\mu^2 = (h_0/l_0)^2$.

A major limitation of Boussinesq-type equations is that they are only applicable to a relatively shallow water depth. For example, to keep errors of the phase velocity estimated

by linearized Boussinesq equations in terms of the depth-averaged velocity within 5% of that determined from the Stokes first-order theory, the water depth has to be less than about one-fifth of the equivalent deep water wavelength (McCowan, 1987). When the velocity on the mean free surface or on the bottom is used in Boussinesq-type equations, the restriction on depth is even more severe. Boussinesq-type equations actually become unstable in the range of short waves or intermediate depths. This behavior poses two difficulties in modelling wave propagation. First, these Boussinesq-type equations can not be used to simulate wave propagation from an intermediate depth to a shallow depth accurately. Secondly, even in the shallow water region numerically generated short waves could cause numerical instabilities and give erroneous results.

Recently, numerous attempts have been made to extend the range of the applicability of Boussinesq-type equations to deep water by improving their linear dispersion characteristics. Witting (1984) used a set of conservative equations to investigate wave propagation in a constant depth channel bounded by two rigid impermeable walls. The depth-averaged and mean free surface velocities used in the Boussinesq-type equations were expanded into a Taylor series in terms of a pseudo velocity. Coefficients in the series were then determined to yield a Padé approximation to the Taylor expansion of the dispersion relation described by the linear Stokes wave theory. Using (2,2) Padé approximation, Witting obtained good results for both short and long waves. However, it is difficult to extend Witting's approach to two horizontal dimensions with a varying depth.

McCowan & Blackman (1989) modified the conventional Boussinesq equations (Peregrine, 1967) by introducing an effective depth and a dispersion tuning parameter. Again, the effective depth and the dispersion tuning parameter were chosen to match the dispersion properties of the first-order Stokes waves. In shallow water the effective depth is identical to the actual depth while in deeper water the effective depth is restricted to the upper part of the water where most of the wave action occurs. Such an approach is, however, only applicable to monochromatic waves and it is not clear if it is applicable to a varying topography.

Madsen & Sorensen (1992) formulated the conventional Boussinesq equations in terms

of depth-integrated velocity components (i.e. fluxes) instead of depth-averaged velocity components. With the mild slope assumption, they included some higher order terms, which were neglected in the process of deriving Boussinesq equations, to the momentum equations and obtained a new form of the Boussinesq equations. Because those additional higher order terms have a common factor B, by choosing a proper value for B, the linear dispersion characteristics of the resulting Boussinesq-type equations can be remarkably improved.

Nwogu (1993a) formally derived an alternative form of the Boussinesq equations using the horizontal velocity on an arbitrary elevation as the velocity variable in the equations. He showed that in the intermediate and deep water, the linear dispersion characteristics of the new set of equations were strongly dependent of the choice of velocity variable. The linear dispersion properties can be significantly improved by selecting a velocity close to mid-depth as the velocity variable. This makes the new set of equations applicable to regular or irregular waves travelling from a relative deep water to a shallow water.

The highest order of spatial derivatives in the equations derived by Nwogu is one order higher than that in the conventional Boussinesq equations (Peregrine, 1967). This creates a difficulty in specifying appropriate boundary conditions and increases the numerical effort for solving these new equations. On the other hand, the parabolic approximation has been developed rapidly as an efficient and practical tool for modelling wave propagation over a varying topography. The parabolic approximation, typically converting an elliptic equation into a parabolic equation, not only reduces the computational efforts dramatically but also alleviates the burden of imposing the down wave boundary conditions, which usually are unknown *a priori* for most coastal hydrodynamic problems. For regular waves consisting of a finite number of harmonics, Liu, Yoon & Kirby (1985) developed the first parabolic approximation model for the conventional Boussinesq equations. In their model waves must propagate in a dominant direction. Therefore, it is a small-angle parabolic approximation model. Recently, Kirby (1990) used the discrete angular spectrum method to develop a wide-angle parabolic model for the conventional Boussinesq equations, in which the topography is allowed to vary only in the on-offshore direction. The approaches used to develop parabolic

models for the conventional Boussinesq equations can not be directly applied to Nwogu's new Boussinesq-type equations, in which the horizontal velocity components and the free surface displacement are coupled together. The reason is that in the process of combining the governing equations into one equation in terms of the free surface displacement the improved dispersion properties can not be preserved.

In this paper, modified Boussinesq equations are derived by employing the velocity potential on an arbitrary elevation instead of horizontal velocity components used in Nwogu's paper. Dispersion properties of the linearized modified Boussinesq equations are compared with those given by the Stokes first-order theory. The optimal elevation of the velocity potential is determined by minimizing the summation of the relative errors of phase and group velocities over a range of water depths from zero to half of the equivalent deep water wavelength. Using the velocity potential on this optimal elevation, the maximum relative errors of phase and group velocities are 1.37% and 6.80%, respectively. Thus, the modified Boussinesq equations can be used to model wave propagation from relative deep water to shallow water. Because the governing equations can be combined into one equation in terms of velocity potential while the improved linear dispersion properties are maintained, we are able to apply the parabolic approximation. For regular waves propagating over a mild-slope topography, a small-angle parabolic approximation model is developed and solved by the pseudospectral Chebyshev method. On the other hand, by assuming that the deviation of the actual water depth from a reference depth (which varies only in the on-offshore direction) is in the same order of magnitude as the typical wave amplitude, the pseudospectral Fourier method used by Chen & Liu (1993) is extended to derive a wide-angle parabolic approximation model for multi-directional wave propagation. The small-angle model is tested by comparing numerical results with the experimental data (Whalin, 1971). Good agreements are observed. The wide-angle model is examined by comparing the model results with the refraction theory of cnoidal waves (Skovgaard & Petersen, 1977) and then is used to study the impact of the directed wave angle on oblique interaction of two identical cnoidal waves propagating over a shallow flat bottom.

2 Derivation of Modified Boussinesq Equations

Consider a wave field bounded by a free surface $z' = \zeta'(x', y', t')$ and a stationary bottom $z' = -h'(x', y')$. A Cartesian coordinate system is adopted, with x'-axis and y'-axis locating on the still water plane and z'-axis pointing vertically upwards. Let h_0, l_0 and a_0 denote the characteristic water depth, wavelength and wave amplitude, respectively. Following dimensionless variables are defined:

$$x = \frac{x'}{l_0} \qquad y = \frac{y'}{l_0} \qquad z = \frac{z'}{h_0} \qquad t = \frac{\sqrt{gh_0}}{l_0} t'$$

$$\zeta = \frac{\zeta'}{a_0} \qquad h = \frac{h'}{h_0} \qquad \Phi = \frac{h_0}{a_0 l_0 \sqrt{gh_0}} \Phi'$$

where g is the gravitational acceleration and Φ is the velocity potential; primes are used to denote dimensional variables.

The dimensionless governing equations and boundary conditions for a potential flow are

$$\mu^2 \nabla^2 \Phi + \frac{\partial^2 \Phi}{\partial z^2} = 0 \qquad -h < z < \varepsilon\zeta \tag{2.1}$$

$$\frac{\partial \Phi}{\partial z} = \mu^2 \left(\frac{\partial \zeta}{\partial t} + \varepsilon \nabla \Phi \cdot \nabla \zeta \right) \qquad \text{at } z = \varepsilon\zeta \tag{2.2}$$

$$\frac{\partial \Phi}{\partial z} = -\mu^2 \nabla \Phi \cdot \nabla h \qquad \text{at } z = -h \tag{2.3}$$

$$\left(\frac{\partial \Phi}{\partial t} + \zeta \right) + \frac{\varepsilon}{2} \left[(\nabla \Phi)^2 + \frac{1}{\mu^2} \left(\frac{\partial \Phi}{\partial z} \right)^2 \right] = 0 \qquad \text{at } z = \varepsilon\zeta \tag{2.4}$$

where $\varepsilon = a_0/h_0$ and $\mu^2 = (h_0/l_0)^2$ are small parameters measuring nonlinearity and frequency dispersion, respectively, and $\nabla = (\frac{\partial}{\partial x}, \frac{\partial}{\partial y})$. We assume that $O(\varepsilon) = O(\mu^2) \ll 1$.

Integrating (2.1) from $z = -h$ to $z = \varepsilon\zeta$ and applying the kinematic boundary conditions (2.2) and (2.3), we obtain

$$\nabla \cdot \left[\int_{-h}^{\varepsilon\zeta} \nabla \Phi \, dz \right] + \frac{\partial \zeta}{\partial t} = 0 \tag{2.5}$$

Expanding the velocity potential Φ as

$$\Phi(x,y,z,t) = \sum_{n=0}^{\infty} \mu^{2n} \Phi_n(x,y,z,t) \tag{2.6}$$

and substituting (2.6) into (2.1) and (2.3), we collect terms with multiplies of like order of even powers of μ

$$\left.\begin{array}{lllll} O(\mu^0): & \frac{\partial^2 \Phi_0}{\partial z^2} = 0 & -h < z < \varepsilon\zeta; & \frac{\partial \Phi_0}{\partial z} = 0 & \text{at } z = -h \\ O(\mu^2): & \frac{\partial^2 \Phi_1}{\partial z^2} = -\nabla^2 \Phi_0 & -h < z < \varepsilon\zeta; & \frac{\partial \Phi_1}{\partial z} = -\nabla \Phi_0 \cdot \nabla h & \text{at } z = -h \\ \vdots & & & & \end{array}\right\} \tag{2.7}$$

The general solution to Φ_n $(n = 0, 1, \ldots)$ in (2.7) can be expressed as

$$\left.\begin{array}{rcl} \Phi_0 &=& \phi_{00}(x,y,t) \\ \Phi_1 &=& \phi_{10}(x,y,t) - z\nabla \cdot (h\nabla\phi_{00}) - \frac{z^2}{2}\nabla^2\phi_{00} \\ \vdots & & \end{array}\right\} \tag{2.8}$$

where $\phi_{00}(x,y,t)$, $\phi_{10}(x,y,t)$, etc. are constants of integration with respect to z. Hence, the expansion (2.6) can be rewritten as

$$\Phi(x,y,z,t) = \phi_{00} + \mu^2 \left[\phi_{10} - z\nabla \cdot (h\nabla\phi_{00}) - \frac{z^2}{2}\nabla^2\phi_{00}\right] + O(\mu^4) \tag{2.9}$$

Denoting $\Phi_\alpha(x,y,t)$ as the potential on an arbitrary elevation $z = z_\alpha(x,y)$, from (2.9) we obtain

$$\begin{aligned} \Phi_\alpha(x,y,t) &= \Phi(x,y,z_\alpha(x,y),t) \\ &= \phi_{00} + \mu^2 \left[\phi_{10} - z_\alpha\nabla \cdot (h\nabla\phi_{00}) - \frac{z_\alpha^2}{2}\nabla^2\phi_{00}\right] + O(\mu^4) \end{aligned} \tag{2.10}$$

Subtracting (2.10) from (2.9) and noting that $\Phi_\alpha = \phi_{00} + O(\mu^2)$, we can express Φ in terms

of Φ_α:

$$\Phi = \Phi_\alpha + \mu^2 \left[(z_\alpha - z)\nabla \cdot (h\nabla\Phi_\alpha) + \frac{1}{2}(z_\alpha^2 - z^2)\nabla^2\Phi_\alpha \right] + O(\mu^4) \tag{2.11}$$

Substituting (2.11) into the mass conservation equation (2.5) and the dynamic free surface boundary condition (2.4) and neglecting $O(\varepsilon\mu^2, \mu^4)$ terms, we obtain a new set of Boussinesq equations, called modified Boussinesq equations, expressed in terms of the free surface displacement ζ and the velocity potential Φ_α on elevation $z = z_\alpha(x, y)$

$$\frac{\partial \zeta}{\partial t} + \nabla \cdot [(\varepsilon\zeta + h)\nabla\Phi_\alpha] + \mu^2 \nabla \cdot \left\{ h\nabla \left[z_\alpha \nabla \cdot (h\nabla\Phi_\alpha) + \frac{z_\alpha^2}{2}\nabla^2\Phi_\alpha \right] + \frac{h^2}{2}\nabla\left[\nabla \cdot (h\nabla\Phi_\alpha)\right] - \frac{h^3}{6}\nabla\nabla^2\Phi_\alpha \right\} = 0 \tag{2.12}$$

$$\frac{\partial \Phi_\alpha}{\partial t} + \zeta + \frac{\varepsilon}{2}(\nabla\Phi_\alpha)^2 + \mu^2 \left[z_\alpha \nabla \cdot \left(h\nabla \frac{\partial \Phi_\alpha}{\partial t} \right) + \frac{z_\alpha^2}{2}\nabla^2 \frac{\partial \Phi_\alpha}{\partial t} \right] = 0 \tag{2.13}$$

From (2.11), the horizontal velocity at $z = z_\alpha$, denoted as $\mathbf{u}_\alpha$, is

$$\mathbf{u}_\alpha = (\nabla\Phi)_{z=z_\alpha} = \nabla\Phi_\alpha + \mu^2 \left[\nabla z_\alpha \nabla \cdot (h\nabla\Phi_\alpha) + z_\alpha \nabla z_\alpha \nabla^2 \Phi_\alpha \right] + O(\mu^4) \tag{2.14}$$

Replacing $\nabla\Phi_\alpha$ by $\mathbf{u}_\alpha$ and noting that $\nabla\Phi_\alpha = \mathbf{u}_\alpha + O(\mu^2)$, we write (2.12) and the gradient of (2.13) in the following form:

$$\frac{\partial \zeta}{\partial t} + \nabla \cdot [(\varepsilon\zeta + h)\mathbf{u}_\alpha] + \mu^2 \nabla \cdot \left\{ \left(\frac{z_\alpha^2}{2} - \frac{h^2}{6} \right) h\nabla(\nabla \cdot \mathbf{u}_\alpha) + \left(z_\alpha + \frac{h}{2} \right) h\nabla\left[\nabla \cdot (h\mathbf{u}_\alpha)\right] \right\} = 0 \tag{2.15}$$

$$\frac{\partial \mathbf{u}_\alpha}{\partial t} + \nabla\zeta + \varepsilon(\mathbf{u}_\alpha \cdot \nabla)\mathbf{u}_\alpha + \mu^2 \left\{ \frac{z_\alpha^2}{2}\nabla \left(\nabla \cdot \frac{\partial \mathbf{u}_\alpha}{\partial t} \right) + z_\alpha \nabla \left[\nabla \cdot \left(h\frac{\partial \mathbf{u}_\alpha}{\partial t} \right) \right] \right\} = 0 \tag{2.16}$$

which is the alternative form of Boussinesq equations derived by Nwogu (1993a), who demonstrated that (2.15) and (2.16) can simulate the nonlinear shoaling, refraction, diffraction and reflection of irregular multi-directional waves from intermediate to shallow water (Nwogu, 1993a,b).

Only two unknowns appear in the modified Boussinesq equations (2.12) and (2.13), Φ_α and ζ, instead of three unknowns when horizontal velocity components are used in (2.15) and (2.16). Furthermore, (2.12) and (2.13) can be combined into one equation in terms of Φ_α. Therefore, in the remaining of this paper we shall carry out analyses and discussions based on (2.12) and (2.13).

3 Discussion about the linear dispersive characteristics

In the case of constant depth, the corresponding linearized dimensional equations of (2.12) and (2.13) become

$$\frac{\partial \zeta}{\partial t} + h\nabla^2\Phi_\alpha + (\alpha + 1/3)h^3\nabla^4\Phi_\alpha = 0 \tag{3.1}$$

$$\frac{\partial \Phi_\alpha}{\partial t} + g\zeta + \alpha h^2\nabla^2\frac{\partial \Phi_\alpha}{\partial t} = 0 \tag{3.2}$$

where $\alpha = \frac{1}{2}(z_\alpha/h)^2 + (z_\alpha/h)$ is a constant.

Consider a small amplitude periodic wave with frequency ω and wave number k, propagating in x-direction:

$$\zeta = a_0 \exp\{i(kx - \omega t)\}, \qquad \Phi_\alpha = \phi_0 \exp\{i(kx - \omega t)\} \tag{3.3}$$

Substituting above expression into (3.1) and (3.2), and letting the discriminant vanish for a non-trivial solution yield the linear dispersion relation as

$$C^2 = \frac{\omega^2}{k^2} = gh\left[\frac{1 - (\alpha + 1/3)(kh)^2}{1 - \alpha(kh)^2}\right] \tag{3.4}$$

where C is the phase velocity. The group velocity, C_g, which is associated with the propagation of wave energy (or wave envelope), is also a very important physical quantity in the process of wave propagation. The group velocity for the linearized modified Boussinesq equations is

given by

$$C_g = \frac{d\omega}{dk} = C\left\{1 - \frac{(kh)^2/3}{[1-\alpha(kh)^2]\,[1-(\alpha+1/3)(kh)^2]}\right\} \tag{3.5}$$

From the Stokes first-order theory, the phase velocity, C_L, and group velocity, C_{gL}, are

$$C_L^2 = \frac{\omega^2}{k_L^2} = gh\frac{\tanh k_L h}{k_L h}; \quad C_{gL} = \frac{d\omega}{dk_L} = \frac{C_L}{2}\left[1 + \frac{2k_L h}{\sinh 2k_L h}\right] \tag{3.6}$$

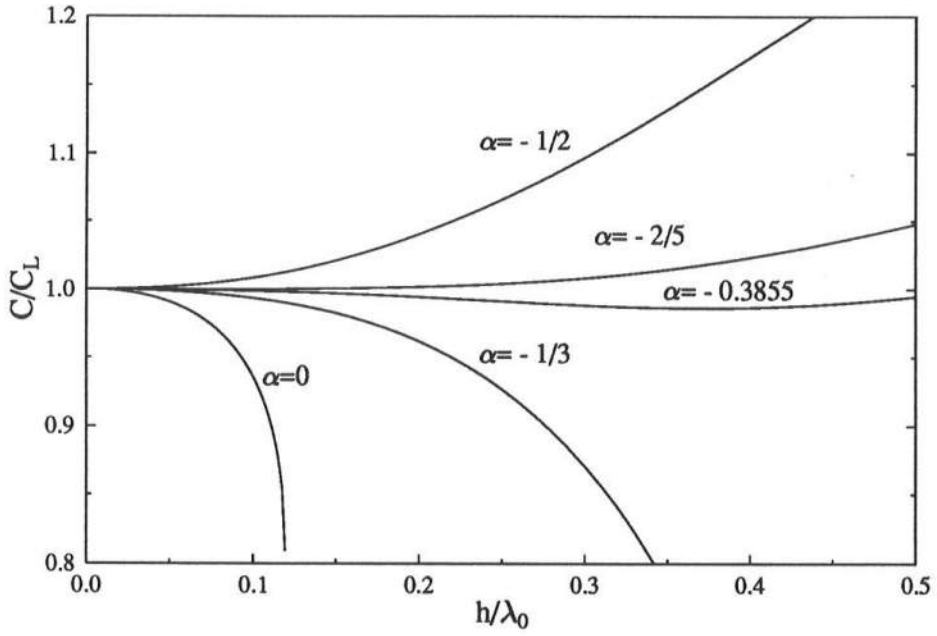

Figure 1: Comparison of normalized phase velocities for different values of α.

The phase velocity C and group velocity C_g ((3.4) and (3.5)) for different values of α, normalized by C_L and C_{gL}, respectively, are plotted as a function of relative depth in figures 1 and 2. The relative depth is defined as the ratio of the water depth, h, to the equivalent deep water wavelength $\lambda_0 = 2\pi g/\omega^2$. The "deep water" depth limit corresponds to $h/\lambda_0 = 0.5$. When the velocity potential on the still water surface ($z_\alpha = 0$) is used in the governing equations, α takes a value of zero. Alternatively, when the velocity potential on seabed ($z_\alpha = -h$) is used, $\alpha = -1/2$. The conventional Boussinesq equations which use the depth-averaged velocity potential (Wu, 1979) corresponds to $\alpha = -1/3$ while $\alpha = -2/5$ represents

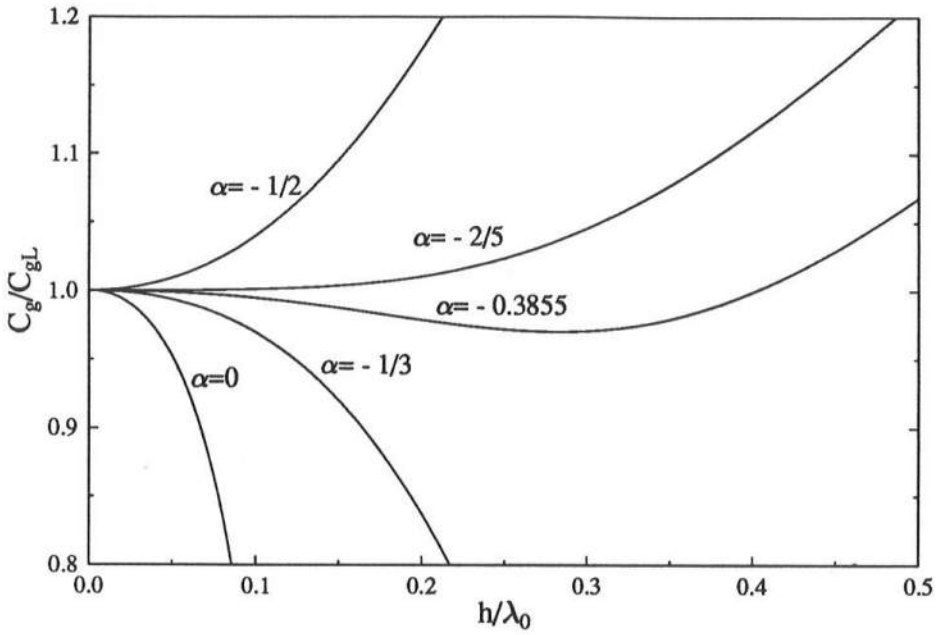

Figure 2: Comparison of normalized group velocities for different values of α.

the Padé approximation to the fourth-order Taylor expansion of $\tanh kh/kh$ in (3.6).

To extend the range of applicability of the modified Boussinesq equations, we define the sum of relative errors of phase and group velocities over the range $0 \leq h/\lambda_0 \leq 0.5$ as

$$I(\alpha) = \int_0^{0.5} \left[(C/C_L - 1)^2 + (C_g/C_{gL} - 1)^2\right] d(h/\lambda_0) \tag{3.7}$$

An optimal value of α for the range $0 \leq h/\lambda_0 \leq 0.5$ is obtained by minimizing $I(\alpha)$. This results in $\alpha = -0.3855$, which corresponds to the elevation $z_\alpha = -0.522h$. The maximum relative errors of phase and group velocities are 1.37% and 6.80%, respectively. Nwogu (1993a) minimized the sum of the relative errors of phase velocity only and determined that $\alpha = -0.390$. Using this α value , Nwogu showed that the maximum relative error in group velocity over the range $0 \leq h/\lambda_0 \leq 0.5$ is 12%.

Figures 1 and 2 show the remarkable improvement of the dispersive characteristics of the modified Boussinesq equations over the conventional Boussinesq equations if the optimal α

value is adopted. Thus, within the linear theory framework the modified Boussinesq equations are applicable to deep water. In other words, they can be extended to the water depth three to five times deeper than the water depth allowable by the conventional Boussinesq equations.

The discussion given above ignores the nonlinearity. Because of the shoaling effect the wave amplitude, hence the nonlinearity, decreases as the depth or μ^2 increase. Therefore, as long as the wave amplitude in the deep water is so small that the weak nonlinearity assumption is still valid when the wave reaches the shallow water region, the modified Boussinesq equations can model wave propagation from deep water to shallow water.

4 Parabolic Approximation

In this section we shall apply the parabolic approximation to the modified Boussinesq equations in the frequency domain to develop both small-angle and wide-angle parabolic models.

Consider regular waves, we can expand Φ_α and ζ as Fourier series in time and then truncate the series:

$$\Phi_\alpha(x,y,t) = \sum_{n=0}^{N} \frac{\phi_n(x,y)}{2} e^{-in\omega t} \; + \; c.c. \tag{4.1}$$

$$\zeta(x,y,t) = \sum_{n=0}^{N} \frac{\zeta_n(x,y)}{2} e^{-in\omega t} \; + \; c.c. \tag{4.2}$$

where *c.c.* represents the complex conjugate.

Substituting (4.1) and (4.2) into (2.12) and (2.13), we obtain

$$\begin{aligned} &-in\omega\zeta_n + \nabla\cdot(h\nabla\phi_n) + \frac{\varepsilon}{2}\nabla\cdot\left\{\sum_{s=1}^{n-1}\zeta_s\nabla\phi_{n-s}\right. \\ &\left. + \sum_{s=1}^{N-n}\left[\bar{\zeta}_s\nabla\phi_{n+s} + \zeta_{n+s}\nabla\bar{\phi}_s\right]\right\} + \mu^2\nabla\cdot\vec{\rho}_n = 0 \end{aligned} \tag{4.3}$$

and

$$\zeta_n = in\omega\phi_n + in\omega\mu^2 f_n - \frac{\varepsilon}{4}\left[\sum_{s=1}^{n-1}\nabla\phi_s\cdot\nabla\phi_{n-s} + 2\sum_{s=1}^{N-n}\nabla\bar{\phi}_s\cdot\nabla\phi_{n+s}\right] \tag{4.4}$$

where $1 \le n \le N$. The zero-th harmonic ϕ_0 has been ignored since it corresponds to a slowly

varying steady state, i.e. $O(\nabla\phi_0) = O(\varepsilon)$. In (4.3) and (4.4) overbar is used to indicate the corresponding complex conjugate and

$$f_n(x,y) = z_\alpha \nabla\cdot(h\nabla\phi_n) + \frac{z_\alpha^2}{2}\nabla^2\phi_n = \alpha h^2\nabla^2\phi_n + z_\alpha \nabla h\cdot\nabla\phi_n \tag{4.5}$$

$$\vec{\rho}_n(x,y) = h\nabla f_n + \frac{h^2}{2}\nabla\left[\nabla\cdot(h\nabla\phi_n)\right] - \frac{h^3}{6}\nabla\nabla^2\phi_n \tag{4.6}$$

To apply the parabolic approximation to (4.3) and (4.4), we first combine these equations into one equation in terms of velocity potential only.

Substituting (4.4) into (4.3) and neglecting $O(\varepsilon^2)$ terms, we obtain:

$$\begin{aligned}\nabla\cdot(h\nabla\phi_n) + n^2\omega^2(\phi_n + \mu^2 f_n) + \mu^2\nabla\cdot\vec{\rho}_n = -in\omega\frac{\varepsilon}{4}\Bigg[\sum_{s=1}^{n-1}\nabla\phi_s\cdot\nabla\phi_{n-s} \\ + 2\sum_{s=1}^{N-n}\nabla\bar{\phi}_s\cdot\nabla\phi_{n+s}\Bigg] - i\omega\frac{\varepsilon}{2}\nabla\cdot\Bigg\{\sum_{s=1}^{n-1}s(\phi_s + \mu^2 f_s)\nabla\phi_{n-s} \\ - \sum_{s=1}^{N-n}\left[s(\bar{\phi}_s + \mu^2\bar{f}_s)\nabla\phi_{n+s} - (n+s)(\phi_{n+s} + \mu^2 f_{n+s})\nabla\bar{\phi}_s\right]\Bigg\}\end{aligned} \tag{4.7}$$

For the n-th harmonic, the linear dispersion relation of (4.7) is

$$\frac{n^2\omega^2}{k_n^2} = h\frac{1-(\alpha+1/3)\mu^2(k_nh)^2}{1-\alpha\mu^2(k_nh)^2} \tag{4.8}$$

When $n = 1$, the dimensional form of (4.8) is exactly the same as (3.4). Therefore, the improved dispersive characteristics of the modified Boussinesq equations with the optimal value of α are preserved. On the other hand, if we eliminate ϕ_n from (4.3) and (4.4) to obtain a combined equation for ζ_n, the corresponding linear dispersion relation is given by (4.8) with $\alpha = 0$, which is worse than the linear dispersion relation of the conventional Boussinesq equations ($\alpha = -1/3$, see figures 1 and 2). In Nwogu's paper (1993a), the alternative form of Boussinesq equations is expressed in terms of horizontal velocity components and the free surface displacement (see (2.15) and (2.16)). If the velocity components are eliminated to obtain one equation for the free surface displacement, the resulting linear dispersion relation

also corresponds to (4.8) with $\alpha = 0$. This is one of the primary reasons why the velocity potential is used in this paper. The parabolic approximation can then be applied to the equation for ϕ_n.

Assume that the topography varies slowly, i.e. $h = h(\varepsilon x, \varepsilon y)$, (4.7) can be further simplified after $O(\varepsilon^2)$ terms have been dropped:

$$\begin{aligned}
&\beta_n \nabla^2 \phi_n + n^2\omega^2\phi_n + (\alpha + 1/3)\mu^2 h^3 \nabla^4 \phi_n = -C_\alpha \mu^2 h^2 \nabla h \cdot \nabla \nabla^2 \phi_n \\
&\quad - \tau_n \nabla h \cdot \nabla \phi_n - i\omega \frac{\varepsilon}{2} \sum_{s=1}^{n-1} s \Big[2\, \nabla \phi_s \cdot \nabla \phi_{n-s} + \alpha \mu^2 h^2 \nabla \nabla^2 \phi_s \cdot \nabla \phi_{n-s} \\
&\quad + (\phi_s + \alpha \mu^2 h^2 \nabla^2 \phi_s) \nabla^2 \phi_{n-s} \Big] - i\omega \frac{\varepsilon}{2} \sum_{s=1}^{N-n} \Big[n(2 \nabla \bar{\phi}_s \cdot \nabla \phi_{n+s} \\
&\quad + \alpha \mu^2 h^2 \nabla^2 \phi_{n+s} \nabla^2 \bar{\phi}_s) - s(\bar{\phi}_s \nabla^2 \phi_{n+s} + \alpha \mu^2 h^2 \nabla \nabla^2 \bar{\phi}_s \cdot \nabla \phi_{n+s}) \\
&\quad + (n+s)(\phi_{n+s} \nabla^2 \bar{\phi}_s + \alpha \mu^2 h^2 \nabla \nabla^2 \phi_{n+s} \cdot \nabla \bar{\phi}_s) \Big] \quad (1 \le n \le N)
\end{aligned} \tag{4.9}$$

where

$$\beta_n = h + \alpha \mu^2 n^2 \omega^2 h^2, \quad \tau_n = 1 + z_\alpha \mu^2 n^2 \omega^2, \quad C_\alpha = 1 + 5\alpha + \sqrt{1 + 2\alpha} \tag{4.10}$$

In (4.9), the last term on the left-hand side and the first term on the right-hand side come from $\mu^2 \nabla \cdot \vec{\rho}_n$ in (4.7). The leading order terms in (4.9), i.e. all terms on the left-hand side, describe the propagation of linear dispersive waves over a constant depth. The frequency dispersion is represented by the coefficient β_n as well as the fourth-order derivative terms on the left-hand side of (4.9). The first two terms on the right-hand side of (4.9) denote the effects of the varying topography, while the rest of terms on the right-hand side are contributed by nonlinearity. We remark that the fourth-order derivative terms vanish in the conventional Boussinesq equations for $\alpha = -1/3$. Once we solve (4.9) for $\phi_n(x, y)$ $(n = 1, \ldots, N)$, the free surface displacement $\zeta_n(x, y)$ $(n = 1, \ldots, N)$ can be computed immediately from (4.4).

4.1 Small-Angle Parabolic Model

To develop a small-angle parabolic model, we assume that the primary wave propagation direction is in x-direction. Rewrite ϕ_n as

$$\phi_n(x,y) = \Psi_n(x,y)e^{i\int K_n(\varepsilon x)dx} \tag{4.11}$$

where $K_n(\varepsilon x)$ is the wave number of the n-th harmonic corresponding to a reference water depth $H(\varepsilon x)$ (If h is a function of x only, $H = h$). The explicit expression of K_n is (from (4.8))

$$K_n^2 = \frac{1+\alpha\mu^2n^2\omega^2H - \sqrt{(1+\alpha\mu^2n^2\omega^2H)^2 - 4(\alpha+1/3)\mu^2n^2\omega^2H}}{2(\alpha+1/3)\mu^2H^2} \tag{4.12}$$

In (4.11) the amplitude function $\Psi_n(x,y)$ varies slowly in both x- and y-direction because of the mild slope assumption. We assume that

$$\frac{\partial^p\Psi_n}{\partial x^p} \sim O(\varepsilon^p), \qquad \frac{\partial^p\Psi_n}{\partial y^p} \sim O(\varepsilon^{p/2}) \qquad (p=1,2,3,4) \tag{4.13}$$

Substituting (4.11) into (4.9), and using

$$\frac{\partial^2\phi_n}{\partial x^2} = \left[(i\frac{dK_n}{dx} - K_n^2)\Psi_n + 2iK_n\frac{\partial\Psi_n}{\partial x}\right]e^{i\int K_n dx} + O(\varepsilon^2) \tag{4.14}$$

$$\frac{\partial^4\phi_n}{\partial x^4} = -\left[(6iK_n^2\frac{dK_n}{dx} - K_n^4)\Psi_n + 4iK_n^3\frac{\partial\Psi_n}{\partial x}\right]e^{i\int K_n dx} + O(\varepsilon^2) \tag{4.15}$$

$$\frac{\partial^4\phi_n}{\partial x^2\partial y^2} = -K_n^2\frac{\partial^2\Psi_n}{\partial y^2}e^{i\int K_n dx} + O(\varepsilon^2) \tag{4.16}$$

we obtain

$$\begin{aligned}\frac{\partial\Psi_n}{\partial x} = \frac{i}{2K_n}\Bigg\{&\frac{\partial^2\Psi_n}{\partial y^2} + \frac{1}{W_n}\Bigg[\left(P_n + iR_nK_n\frac{\partial h}{\partial x}\right)\Psi_n + R_n\frac{\partial h}{\partial y}\frac{\partial\Psi_n}{\partial y} \\ &+ i\omega\frac{\varepsilon}{2}\left(\sum_{s=1}^{n-1}\sigma_{ns}\Psi_s\Psi_{n-s} + \sum_{s=1}^{N-n}\gamma_{ns}\overline{\Psi}_s\Psi_{n+s}\right)\Bigg]\Bigg\}\end{aligned} \tag{4.17}$$

where

$$W_n = \beta_n - 2(\alpha + 1/3)\mu^2 h^3 K_n^2 \tag{4.18}$$

$$R_n = \tau_n - C_\alpha \mu^2 h^2 K_n^2 \tag{4.19}$$

$$P_n = -\beta_n K_n^2 + n^2\omega^2 + (\alpha + 1/3)\mu^2 h^3 K_n^4 + i\left[\beta_n - 6(\alpha + 1/3)\mu^2 h^3 K_n^2\right]\frac{dK_n}{dx} \tag{4.20}$$

$$\sigma_{ns} = sK_{n-s}e^{i\int(K_s + K_{n-s} - K_n)dx}\left[\alpha\mu^2 h^2 K_s^2(K_s + K_{n-s}) - (2K_s + K_{n-s})\right] \tag{4.21}$$

$$\begin{aligned}\gamma_{ns} = e^{i\int(K_{n+s} - K_s - K_n)dx}&\left[nK_sK_{n+s}(2 + \alpha\mu^2 h^2 K_s K_{n+s})\right.\\ &\left. + sK_{n+s}(K_{n+s} + \alpha\mu^2 h^2 K_s^3) - (n+s)K_s(K_s + \alpha\mu^2 h^2 K_{n+s}^3)\right]\end{aligned} \tag{4.22}$$

In the dimensional form, (4.17) becomes (after primes have been dropped)

$$\begin{aligned}\frac{\partial\Psi_n}{\partial x} = \frac{i}{2K_n}&\left\{\frac{\partial^2\Psi_n}{\partial y^2} + \frac{1}{W_n}\left[\left(P_n + iR_nK_n\frac{\partial h}{\partial x}\right)\Psi_n + R_n\frac{\partial h}{\partial y}\frac{\partial\Psi_n}{\partial y}\right.\right.\\ &\left.\left. + \frac{i\omega}{2g}\left(\sum_{s=1}^{n-1}\sigma_{ns}\Psi_s\Psi_{n-s} + \sum_{s=1}^{N-n}\gamma_{ns}\overline{\Psi}_s\Psi_{n+s}\right)\right]\right\} \quad (1 \le n \le N)\end{aligned} \tag{4.23}$$

The corresponding dimensional forms for $\beta_n, \tau_n, \sigma_{ns}, \gamma_{ns}, K_n, W_n, P_n$ and R_n are given in appendix A.

We reiterate here that the amplitude function $\Psi_n(x,y)$ has been assumed to be $O(1)$ and to be a slowly varying function of x and y. Therefore, the phase functions appeared in the coefficients of the nonlinear terms in (4.17), σ_{ns} and γ_{ns}, must also vary slowly, i.e. the integrands in the expressions of σ_{ns} and γ_{ns}, (4.21) and (4.22), must be small. Hence, a nearly triad resonance is anticipated. For instance, if only two harmonics are considered, in the governing equation for Ψ_2 the forcing term on the right-hand side of (4.17), $i\omega\varepsilon\sigma_{21}\Psi_1^2/2$, is generated by the self interaction of the first harmonic. The integrand in σ_{21} is $2K_1 - K_2$, which indeed is the phase mismatch between the bound and free second harmonic wave numbers. In the shallow water, the phase mismatch is small (from (4.12)). However, in intermediate depths, the mismatch becomes large, and the assumption (4.13) for the second harmonic is

not valid. A special treatment for this situation is presented in section 5.1.

After solving (4.17) for $\Psi_n(x,y)$ $(n = 1,\ldots,N)$, we can obtain free surface displacement $\zeta_n(x,y)$ up to $O(\varepsilon)$ by substituting (4.11) and (4.14) into (4.4).

$$\begin{aligned}\zeta_n e^{-i\int K_n dx} = {} & in\omega\Psi_n + in\omega\mu^2\left\{\alpha h^2\left[\left(i\frac{dK_n}{dx} - K_n^2\right)\Psi_n + 2iK_n\frac{\partial\Psi_n}{\partial x} + \frac{\partial^2\Psi_n}{\partial y^2}\right]\right. \\ & \left. + z_\alpha\left(iK_n\Psi_n\frac{\partial h}{\partial x} + \frac{\partial h}{\partial y}\frac{\partial\Psi_n}{\partial y}\right)\right\} + \frac{\varepsilon}{4}\left[\sum_{s=1}^{n-1} K_s K_{n-s}\Psi_s\Psi_{n-s}e^{i\int(K_s+K_{n-s}-K_n)dx}\right. \\ & \left. - 2\sum_{s=1}^{N-n} K_s K_{n+s}\overline{\Psi}_s\Psi_{n+s}e^{i\int(K_{n+s}-K_s-K_n)dx}\right] \qquad (1\le n\le N)\end{aligned} \tag{4.24}$$

The dimensional form of the above expression is also given in appendix A.

For waves propagating within a channel bounded by two parallel vertical walls, we apply the pseudospectral Chebyshev method to solve (4.23). Details are given in appendix B.

4.2 Wide-Angle Parabolic Model

To develop a wide-angle model for multi-directional wave propagation, first we apply the pseudospectral Fourier method to decompose the wave field into a series of modes including all the discrete forward and backward propagation modes (Chen & Liu, 1993).

Equation (4.9) can be rewritten as

$$B_n\nabla^2\phi_n + n^2\omega^2\phi_n + (\alpha + 1/3)\mu^2 H^3\nabla^4\phi_n = -U_n - i\omega\frac{\varepsilon}{2}V_n \tag{4.25}$$

where

$$B_n = H + \alpha\mu^2 n^2\omega^2 H^2 \tag{4.26}$$

$$\begin{aligned}U_n = {} & (\beta_n - B_n)\nabla^2\phi_n + (\alpha + 1/3)\mu^2(h^3 - H^3)\nabla^4\phi_n \\ & + C_\alpha\mu^2 h^2\nabla h\cdot\nabla\nabla^2\phi_n + \tau_n\nabla h\cdot\nabla\phi_n\end{aligned} \tag{4.27}$$

$$V_n = \sum_{s=1}^{n-1} s \left[2\,\nabla\phi_s \cdot \nabla\phi_{n-s} + \alpha\mu^2 h^2 \nabla\nabla^2\phi_s \cdot \nabla\phi_{n-s} + (\phi_s + \alpha\mu^2 h^2 \nabla^2\phi_s) \right.$$
$$\left. \nabla^2\phi_{n-s} \right] + \sum_{s=1}^{N-n} \left[n(2\nabla\bar{\phi}_s \cdot \nabla\phi_{n+s} + \alpha\mu^2 h^2 \nabla^2\phi_{n+s} \nabla^2\bar{\phi}_s) - s(\bar{\phi}_s \nabla^2\phi_{n+s} + \right.$$
$$\left. \alpha\mu^2 h^2 \nabla\nabla^2\bar{\phi}_s \cdot \nabla\phi_{n+s}) + (n+s)(\phi_{n+s} \nabla^2\bar{\phi}_s + \alpha\mu^2 h^2 \nabla\nabla^2\phi_{n+s} \cdot \nabla\bar{\phi}_s) \right] \qquad (4.28)$$

We assume that the wave field in the along-shore direction (y-direction) is periodic with a period L. After a linear transformation from interval $y \in [0, L]$ to $\tilde{y} \in [0, 2\pi]$ is taken, (4.25) becomes

$$B_n \left[\frac{\partial^2\phi_n}{\partial x^2} + \Lambda_0 \frac{\partial^2\phi_n}{\partial\tilde{y}^2} \right] + n^2\omega^2\phi_n + (\alpha + 1/3)\mu^2 H^3$$
$$\left[\frac{\partial^4\phi_n}{\partial x^4} + 2\Lambda_0 \frac{\partial^4\phi_n}{\partial x^2 \partial\tilde{y}^2} + \Lambda_0^2 \frac{\partial^4\phi_n}{\partial\tilde{y}^4} \right] = -U_n - i\omega\frac{\varepsilon}{2} V_n \qquad (4.29)$$

where

$$\Lambda_0 = (2\pi/L)^2$$

Now we use trigonometric polynomials to interpolate $\phi_n(x, \tilde{y})$ in $\tilde{y}$-direction at the following set of collocation points (Gottlieb et al. 1984):

$$\tilde{y}_j = \frac{\pi j}{M} \qquad (0 \le j \le 2M-1) \qquad (4.30)$$

$$\phi_n(x, \tilde{y}) = \sum_{j=0}^{2M-1} g_j(\tilde{y}) \phi_n^j(x) \qquad (4.31)$$

where

$$\phi_n^j(x) = \phi_n(x, \tilde{y}_j); \quad g_j(\tilde{y}) = \frac{1}{2M} \sin[M(\tilde{y} - \tilde{y}_j)] \cot(\frac{\tilde{y} - \tilde{y}_j}{2}) \qquad (4.32)$$

The interpolant $g_j(\tilde{y})\,(0 \le j \le 2M-1)$ are trigonometric polynomials of degree M and at each collocation point $\tilde{y}_m$, $g_j(\tilde{y}_m) = \delta_{jm}$. The p-th order derivative of $\phi_n(x, \tilde{y})$ with respect to

$\tilde{y}$, evaluated at the collocation $\tilde{y} = \tilde{y}_m$ is given by

$$\left.\frac{\partial^p \phi_n(x,\tilde{y})}{\partial \tilde{y}^p}\right|_{\tilde{y}=\tilde{y}_m} = \sum_{j=0}^{2M-1} \phi_n^j(x) \left.\frac{d^p g_j(\tilde{y})}{d\tilde{y}^p}\right|_{\tilde{y}=\tilde{y}_m} = \sum_{j=0}^{2M-1} [D_p]_{mj} \phi_n^j(x) \tag{4.33}$$

where

$$[D_p]_{mj} = \left.\frac{d^p g_j(\tilde{y})}{d\tilde{y}^p}\right|_{\tilde{y}=\tilde{y}_m} \tag{4.34}$$

which is a $2M \times 2M$ matrix. Specifically

$$[D_1]_{mj} = \begin{cases} \frac{1}{2}(-1)^{m+j} \cot(\frac{\tilde{y}_m - \tilde{y}_j}{2}), & j \neq m \\ 0, & j = m \end{cases} \tag{4.35}$$

and

$$[D_2]_{mj} = \begin{cases} \frac{1}{2}(-1)^{m+j+1} \csc^2(\frac{\tilde{y}_m - \tilde{y}_j}{2}), & j \neq m \\ -\frac{2M^2+1}{6}, & j = m \end{cases} \tag{4.36}$$

When $p > 2$, the p-th order spectral differentiation matrix D_p can be written as a power of D_2 if p is even and as a power of D_1 (or D_1 times a power of D_2) if p is odd.

From (4.35) and (4.36), D_1 is a real anti-symmetric matrix and D_2 is a real symmetric matrix. Hence, D_{2p} is also a real symmetric while D_{2p+1} is a real anti-symmetric matrix for $p \geq 1$.

Substituting (4.31) and (4.33) into (4.29) and evaluating the resulting equation at each collocation point $\tilde{y} = \tilde{y}_m$ $(0 \leq m \leq 2M-1)$, we obtain

$$\begin{aligned} B_n \left\{ \frac{d^2\phi_n^m}{dx^2} + \Lambda_0 \sum_{j=0}^{2M-1} [D_2]_{mj} \phi_n^j \right\} + n^2\omega^2 \phi_n^m + (\alpha + 1/3)\mu^2 H^3 \left\{ \frac{d^4\phi_n^m}{dx^4} \right. \\ \left. + 2\,\Lambda_0 \sum_{j=0}^{2M-1} [D_2]_{mj} \frac{d^2\phi_n^j}{dx^2} + \Lambda_0^2 \sum_{j=0}^{2M-1} [D_4]_{mj} \phi_n^j \right\} = -U_n^m - i\omega \frac{\varepsilon}{2} V_n^m \end{aligned} \tag{4.37}$$

where the superscript m denotes that the corresponding variable is evaluated at $\tilde{y} = \tilde{y}_m$.

Because D_2 is symmetric, there exists an orthogonal matrix Q such that

$$Q^T D_2 Q = I\left\{-\lambda^2/\Lambda_0\right\} \tag{4.38}$$

where I is the $2M \times 2M$ identity matrix and the $2M$ column vector $\{-\lambda^2/\Lambda_0\}$ is the spectrum of D_2, i.e. its l-th $(0 \leq l \leq 2M-1)$ entry $-\lambda_l^2/\Lambda_0$ is the eigenvalue of D_2. The transformation matrix Q and the spectrum of D_2 can be given analytically (Chen & Liu, 1993).

To decompose the wave field into a series of modes including all discrete forward and backward propagation modes, we introduce following transformation

$$\phi_n^m(x) = \sum_{q=0}^{2M-1} Q_{mq}\eta_n^q(x) \qquad (0 \leq m \leq 2M-1) \tag{4.39}$$

Substituting (4.39) into (4.37), multiplying the resulting equation by Q_{ml} and summing m from 0 to $2M-1$, we obtain

$$B_n\left[\frac{d^2\eta_n^l}{dx^2} - \lambda_l^2\eta_n^l\right] + n^2\omega^2\eta_n^l + (\alpha + 1/3)\mu^2 H^3\left[\frac{d^4\eta_n^l}{dx^4} - 2\lambda_l^2\frac{d^2\eta_n^l}{dx^2}\right.$$
$$\left. + \lambda_l^4\eta_n^l\right] = -\sum_{m=0}^{2M-1} Q_{ml}\left[U_n^m + i\omega\frac{\varepsilon}{2}V_n^m\right] \qquad (0 \leq l \leq 2M-1) \tag{4.40}$$

in which the orthogonality of Q and

$$Q^T D_4 Q = Q^T D_2 Q Q^T D_2 Q = I\left\{-\lambda^4/{\Lambda_0}^2\right\}, \tag{4.41}$$

from (4.38) have been used.

To apply the parabolic approximation to (4.40), we impose another assumption for the topography: $(h - H) \sim O(\varepsilon)$, i.e. the deviation of the actual depth from the reference depth is in the same order of magnitude as the typical wave amplitude, then all the terms on the right-hand side of (4.40) have the same order magnitude of $O(\varepsilon)$.

Solutions to (4.40) contain both forward and backward propagation fields. In the present study we assume that the backward propagation field is negligible. Consequently, η_n^l represents

a forward propagation mode whose wave number component in the x-direction is $\sqrt{K_n^2-\lambda_l^2}$ and propagation direction is $\tan^{-1}(\lambda_l/\sqrt{K_n^2-\lambda_l^2})$ measured from $+x$-direction. Therefore, η_n^l can be expressed as

$$\eta_n^l(x) = \psi_n^l(x) e^{i\int\sqrt{K_n^2-\lambda_l^2}\,dx} \tag{4.42}$$

with

$$\frac{d^p\psi_n^l}{dx^p} \sim O(\varepsilon^p) \qquad (p=1,2,3,4) \tag{4.43}$$

Substituting (4.42) into (4.40) and noting that

$$\frac{d^2\eta_n^l}{dx^2} = \left\{\left[\frac{i}{2\sqrt{K_n^2-\lambda_l^2}}\frac{dK_n^2}{dx} - (K_n^2-\lambda_l^2)\right]\psi_n^l + 2i\sqrt{K_n^2-\lambda_l^2}\frac{d\psi_n^l}{dx}\right\} e^{i\int\sqrt{K_n^2-\lambda_l^2}\,dx} + O(\varepsilon^2)$$

$$\frac{d^3\eta_n^l}{dx^3} = -\left\{\left[\frac{3}{2}\frac{dK_n^2}{dx} + i(K_n^2-\lambda_l^2)^{3/2}\right]\psi_n^l + 3(K_n^2-\lambda_l^2)\frac{d\psi_n^l}{dx}\right\} e^{i\int\sqrt{K_n^2-\lambda_l^2}\,dx} + O(\varepsilon^2)$$

$$\begin{aligned}\frac{d^4\eta_n^l}{dx^4} = \Bigg\{&\left[-3i\sqrt{K_n^2-\lambda_l^2}\frac{dK_n^2}{dx} + (K_n^2-\lambda_l^2)^2\right]\psi_n^l \\ &- 4i(K_n^2-\lambda_l^2)^{3/2}\frac{d\psi_n^l}{dx}\Bigg\} e^{i\int\sqrt{K_n^2-\lambda_l^2}\,dx} + O(\varepsilon^2)\end{aligned}$$

we have

$$\begin{aligned}&\frac{i}{2\sqrt{K_n^2-\lambda_l^2}}\left[B_n - 2(\alpha+1/3)\mu^2H^3(3K_n^2-2\lambda_l^2)\right]\frac{dK_n^2}{dx}\eta_n^l + 2i\sqrt{K_n^2-\lambda_l^2}\,[B_n - \\ &2(\alpha+1/3)\mu^2H^3K_n^2]\left[\frac{d\eta_n^l}{dx} - i\sqrt{K_n^2-\lambda_l^2}\,\eta_n^l\right] = -\sum_{m=0}^{2M-1} Q_{ml}\left[U_n^m + i\omega\frac{\varepsilon}{2}V_n^m\right]\end{aligned} \tag{4.44}$$

where

$$-B_nK_n^2 + n^2\omega^2 + (\alpha+1/3)\mu^2H^3K_n^4 = 0$$

from (4.12) and

$$\frac{d\psi_n^l}{dx}e^{i\int\sqrt{K_n^2-\lambda_l^2}\,dx} = \frac{d\eta_n^l}{dx} - i\sqrt{K_n^2-\lambda_l^2}\,\eta_n^l$$

have been used.

In the expression of $U_n + i\omega\varepsilon V_n/2$ (see (4.27) and (4.28)), the order of magnitude of all known coefficients is $O(\varepsilon)$. Therefore, $d^p\phi_n^m/dx^p$ appearing in the expression of $U_n^m + i\omega\varepsilon V_n^m/2$ can be approximated as

$$\frac{d\phi_n^m}{dx} = \sum_{q=0}^{2M-1} Q_{mq}\frac{d\eta_n^q}{dx} \approx \sum_{q=0}^{2M-1} i\sqrt{K_n^2 - \lambda_q^2}\, Q_{mq}\eta_n^q \tag{4.45}$$

$$\frac{d^2\phi_n^m}{dx^2} = \sum_{q=0}^{2M-1} Q_{mq}\frac{d^2\eta_n^q}{dx^2} \approx -\sum_{q=0}^{2M-1} (K_n^2 - \lambda_q^2)\, Q_{mq}\eta_n^q \tag{4.46}$$

$$\frac{d^3\phi_n^m}{dx^3} = \sum_{q=0}^{2M-1} Q_{mq}\frac{d^3\eta_n^q}{dx^3} \approx -\sum_{q=0}^{2M-1} i(K_n^2 - \lambda_q^2)^{3/2}\, Q_{mq}\eta_n^q \tag{4.47}$$

$$\frac{d^4\phi_n^m}{dx^4} = \sum_{q=0}^{2M-1} Q_{mq}\frac{d^4\eta_n^q}{dx^4} \approx \sum_{q=0}^{2M-1} (K_n^2 - \lambda_q^2)^2\, Q_{mq}\eta_n^q \tag{4.48}$$

Now terms on the right-hand side of (4.44) can be expressed in terms of $\eta_n^q (0 \le q \le 2M - 1; 1 \le n \le N)$ and do not involve the derivatives of η_n^q. The explicit expressions of U_n^m and V_n^m in terms of η_n^q are given in appendix A.

Equation (4.44) can be written as

$$\begin{aligned}\frac{d\eta_n^l}{dx} = &\left[i\sqrt{K_n^2 - \lambda_l^2} - \frac{1}{4(K_n^2 - \lambda_l^2)}\frac{E_{nl}}{D_n}\frac{dK_n^2}{dx}\right]\eta_n^l \\ &+ \frac{i}{2D_n\sqrt{K_n^2 - \lambda_l^2}}\sum_{m=0}^{2M-1} Q_{ml}\left[U_n^m + i\omega\frac{\varepsilon}{2}V_n^m\right]\end{aligned} \tag{4.49}$$

where

$$D_n = B_n - 2(\alpha + 1/3)\mu^2 H^3 K_n^2 \tag{4.50}$$

$$E_{nl} = B_n - 2(\alpha + 1/3)\mu^2 H^3(3K_n^2 - 2\lambda_l^2) \tag{4.51}$$

In the dimensional form, (4.49) becomes

$$\frac{d\eta_n^l}{dx} = \left[i\sqrt{K_n^2 - \lambda_l^2} - \frac{1}{4(K_n^2 - \lambda_l^2)}\frac{E_{nl}}{D_n}\frac{dK_n^2}{dx}\right]\eta_n^l$$

$$+\frac{i}{2D_n\sqrt{K_n^2-\lambda_l^2}}\sum_{m=0}^{2M-1}Q_{ml}\left[U_n^m+\frac{i\omega}{2g}V_n^m\right] \tag{4.52}$$

The corresponding dimensional forms for B_n,D_n and E_{nl} are given in appendix A.

By solving (4.52) for $\eta_n^l(x)$ $(0 \le l \le 2M-1; 1 \le n \le N)$, we can find the velocity potential for each harmonic $\phi_n(x,y)$ from (4.39) and the corresponding free surface elevation $\zeta_n(x,y)$ from (4.4) $(n = 1, \ldots, N)$.

5 Numerical Examples

Several numerical examples are given in this section to demonstrate the applicability of the modified Boussinesq equations as well as the parabolic approximation models. For all numerical examples, the optimal value of $\alpha = -0.3855$ is used.

5.1 Small-angle parabolic model

Whalin (1971) conducted a series of laboratory experiments concerning wave focusing over a slowly varying topography. The wave tank was $25.603m$ long and $6.096m$ wide. In the middle portion of the wave tank $7.622m < x < 15.242m$, eleven semicircular steps were evenly spaced and led to the shallower portion of the channel.

The equation approximating the topography is given as follows (Whalin, 1971)

$$h(x,y) = \begin{cases} 0.4572 & (0 \le x \le 10.67 - G) \\ 0.4572 + \frac{1}{25}(10.67 - G - x) & (10.67 - G \le x \le 18.29 - G) \\ 0.1524 & (18.29 - G \le x \le 21.34) \end{cases} \tag{5.1}$$

where

$$G(y) = [y(6.096 - y)]^{1/2} \qquad (0 \le y \le 6.096) \tag{5.2}$$

In both (5.1) and (5.2), the length variables are measured in meters. The bottom topography is symmetric with respect to the centerline of the wave tank $y = 3.048m$. A wavemaker was

installed at the deeper portion of the channel where the water depth is $0.4572m$. Three sets of experiments were conducted for periods $T = 1.0s, 2.0s$ and $3.0s$ respectively. Different wave amplitude was generated for each wave period (table 1).

T(s)	$a_0(m)$	$\varepsilon_0 = a_0/h_0$	$\varepsilon_1 = a_0/h_1$	h_0/λ_1	h_0/λ_N
1.0	0.0097	0.0212	0.0636	0.2931	1.1725 ($N = 2$)
	0.0195	0.0427	0.1280		
2.0	0.0075	0.0164	0.0492	0.0733	0.6595 ($N = 3$)
	0.0106	0.0232	0.0696		
	0.0149	0.0326	0.0978		
3.0	0.0068	0.0149	0.0446	0.0326	0.8142 ($N = 5$)
	0.0098	0.0214	0.0643		
	0.0146	0.0319	0.0958		

Table 1: h_0 and h_1 are the water depths in the deeper and shallower portion of the channel, respectively. $\lambda_n = \frac{gT^2}{2\pi n^2}$ is the equivalent deep water wavelength for the n-th harmonic.

Because of the symmetry of the problem with respect to the centerline of the wave tank, the computational domain only consists of one half of the wave tank. The computational domain in x-direction starts from the wavemaker $x = 0$ and ends at $x = 25m$. The no-flux boundary conditions are used along the side-wall and the centerline of the wave tank, i.e.

$$\frac{\partial \phi_n}{\partial y} = 0; \quad \text{along} \quad y = 0,\ 3.048m \tag{5.3}$$

for $1 \leq n \leq N$. The wave amplitude for the first harmonic at the wavemaker ($x = 0$) is prescribed with the values shown in table 1. The initial condition for velocity potential of the first harmonic can be obtained from the free surface elevation by using (3.2)

$$\phi_1(0, y) = \frac{g}{i\omega[1 - \alpha(h_0 k_1)^2]} \zeta_1(0, y) \tag{5.4}$$

where $h_0 = 0.4572m$ is the water depth at $x = 0$ and k_1 is the incident wave number for the first harmonic wave component. The initial conditions for higher harmonics are zero. The

reference depth $H(x)$ is chosen as follows:

$$H(x) = \begin{cases} 0.4572 & (0 \leq x \leq 7.622) \\ 0.4572 + \frac{1}{25}(7.622 - x) & (7.622 \leq x \leq 15.242) \\ 0.1524 & (15.242 \leq x \leq 21.34) \end{cases} \tag{5.5}$$

which indeed is the water depth along the centerline of the wave tank.

In numerical computations, different harmonics, marching steps and collocation points are tested. Numerical results for $T = 2.0s$ and $3.0s$ presented here are obtained by using following computational parameters: number of collocation points $M = 6$ (i.e. $\Delta y = 0.508m$), marching step length $\Delta x = 1/3m$; five harmonics $N = 5$ for $T = 3.0s$ and three harmonics $N = 3$ for $T = 2.0s$.

According to Whalin's (1971) report, the second and third harmonics grow rapidly in the focal zone. This phenomenon was also observed in several mathematical models. Using the Stokes second-order theory, Liu & Tsay (1984) derived a model equation, which is a nonlinear Schrödinger equation with variable coefficients. They produced numerical results for wave period of 1 and 2 seconds. Because the Stokes second-order waves theory was used, their model was unable to obtain more than two harmonics and was not valid in shallow water. Liu, Yoon & Kirby (1985) discussed two models for nonlinear refraction-diffraction of waves in shallow water: the conventional Boussinesq equations and the K-P equation (Kadomtsev & Petviashvili,1970). They presented numerical results for wave period of 3 seconds. These two models are restricted to shallow water and can not be extended to deal with intermediate depth cases where $T = 1.0s$ and $2.0s$. Solving conventional Boussinesq equations directly with a line by line iterative method, Rygg (1988) compared his numerical results with Whalin's experimental data for the cases of $T = 2.0s$ and $3.0s$. Using finite difference methods in time domain, Madsen & Sorensen (1992) and Nwogu (1993b) claimed that the new form of Boussinesq equations they derived are able to simulate all cases in Whalin's experiments.

The small-angle parabolic model is applied to all three cases from intermediate to shallow depth: $T = 1.0, 2.0$ and 3.0 seconds. Figures 3,4 and 5 compare present numerical results

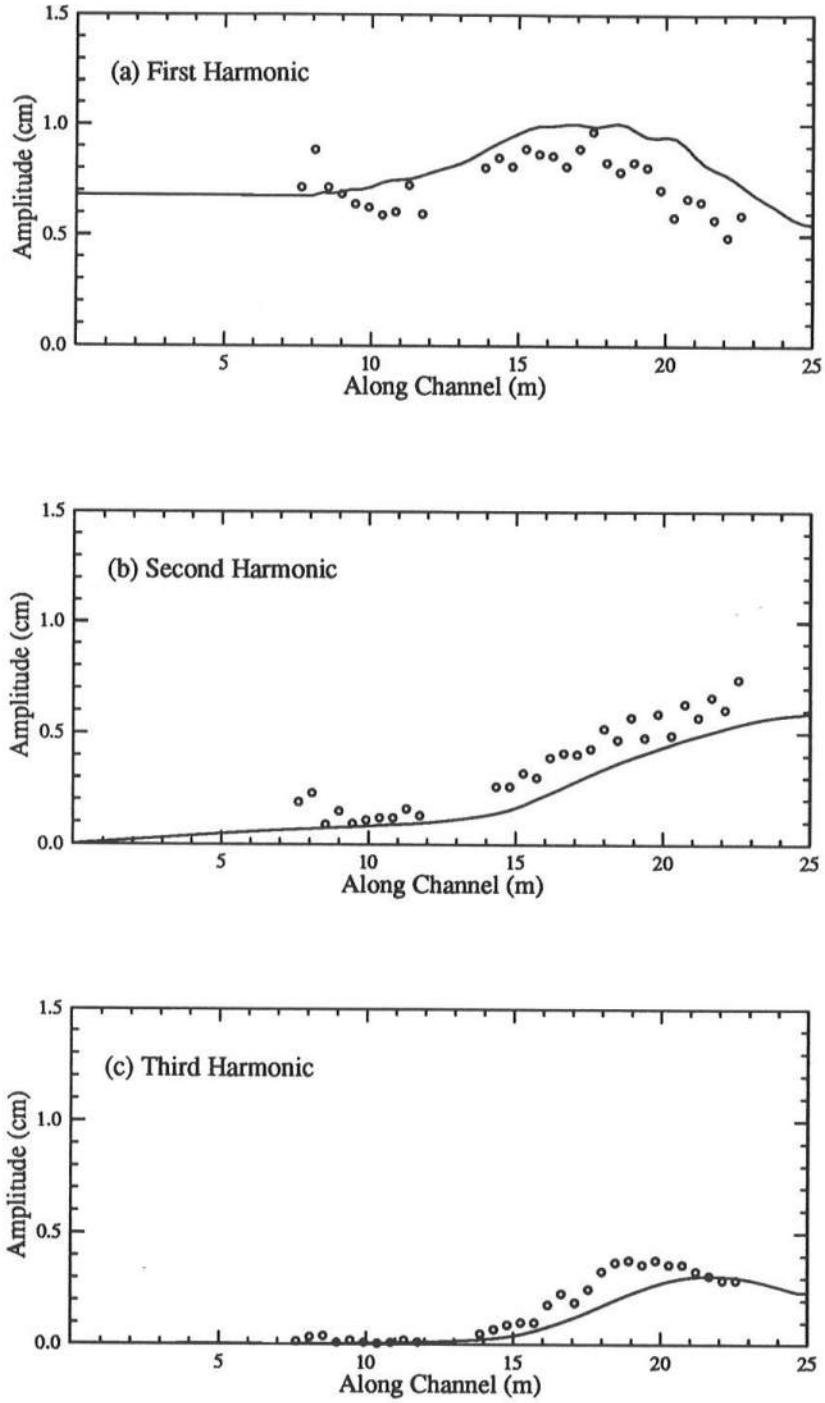

Figure 3: Wave amplitude along the centerline of the wave tank for $T = 3.0s$ and $a_0 = 0.68cm$: —— numerical results (small-angle model); o o o experimental data (Whalin, 1971).

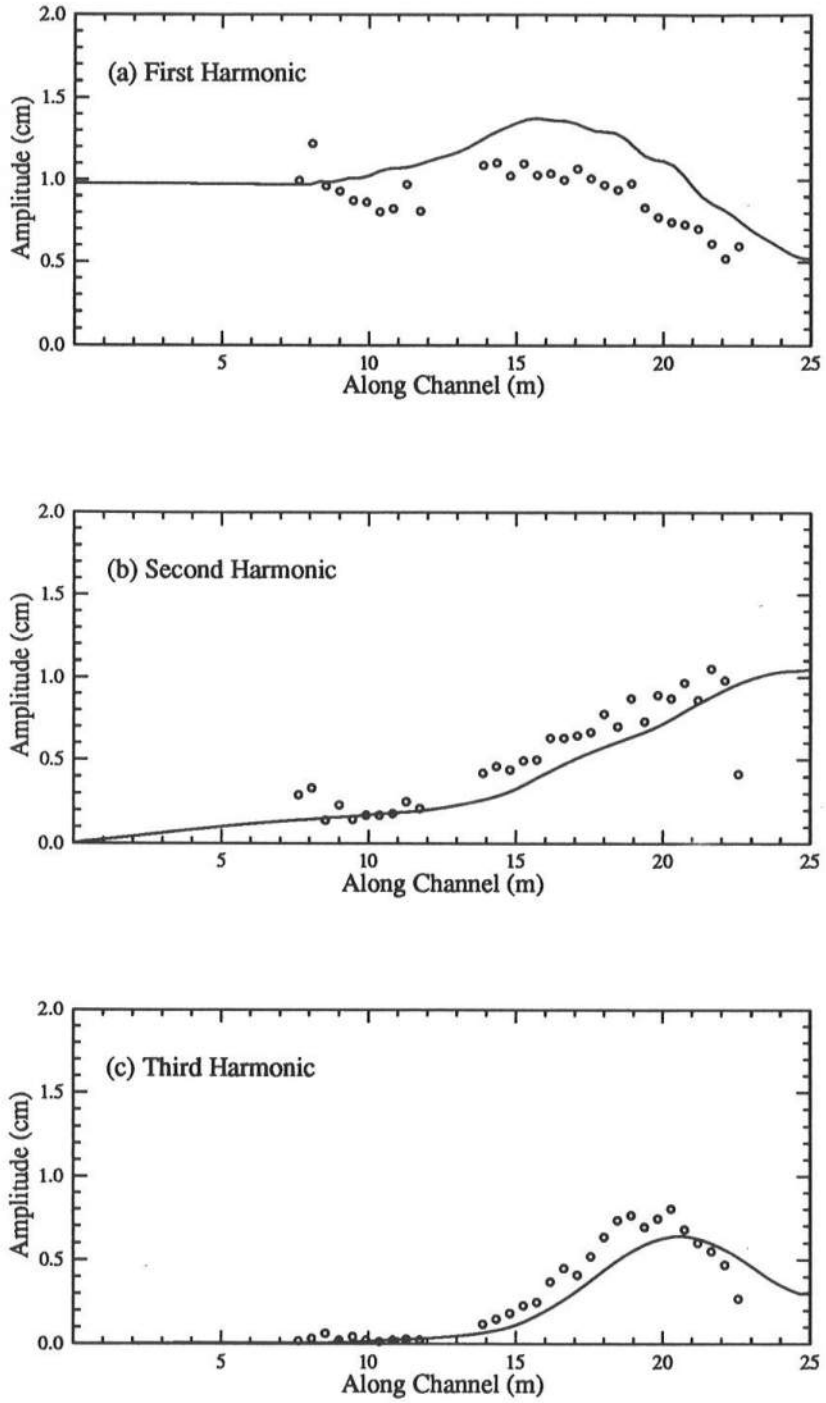

Figure 4: Wave amplitude along the centerline of the wave tank for $T = 3.0s$ and $a_0 = 0.98cm$: —— numerical results (small-angle model); o o o experimental data (Whalin, 1971).

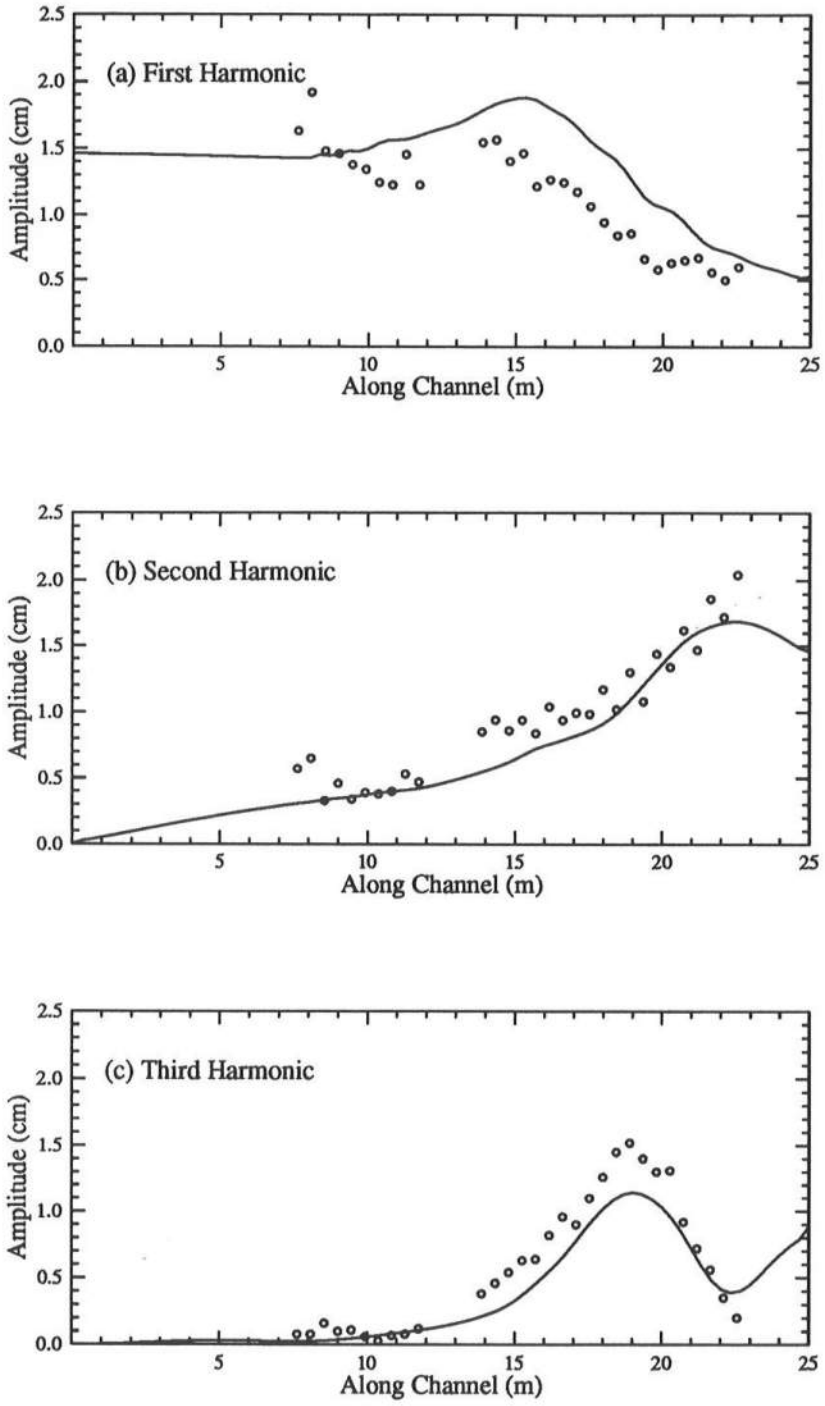

Figure 5: Wave amplitude along the centerline of the wave tank for $T = 3.0s$ and $a_0 = 1.46cm$: —— numerical results (small-angle model); o o o experimental data (Whalin, 1971).

for wave period $T = 3.0s$ with experimental data. Numerical results slightly underpredict the second and third harmonic wave amplitude along the centerline of the wave tank while overpredict the first harmonic wave amplitude. It is worth mentioning that although the relative depth of the free fifth harmonic in the deeper portion of the channel $h_0/\lambda_5 = 0.8142$ (see table 1. $\lambda_N = gT^2/2\pi N^2$, by definition, is the deep water wavelength for the free N-th harmonic) is beyond the range [0, 0.5], the contribution from the fifth harmonic in the deeper portion is almost null. Only in the shallower portion of the channel, where $h_1 = 0.1524m$ and the relative depth of the free fifth harmonic h_1/λ_5 is still within the range [0, 0.5], does the fifth harmonic have a small contribution.

Figures 6,7 and 8 show the comparison between numerical results for wave period $T = 2.0s$ with experimental data. For $a_0 = 0.75cm$ and $1.06cm$ (figures 6 and 7), numerical results agree very well with experimental data, especially in the focal zone. From figures 3–8, in spite of the scattering in the experimental data we may conclude that the small-angle parabolic model gives a very good prediction of the first, second and third harmonic wave amplitude along the centerline for $T = 2.0s$ and $3.0s$.

For cases of $T = 1.0s$, only two harmonics are considered. The relative depth of the incident wave, $h_0/\lambda_1 = 0.2913$ (see table 1), is in the intermediate depth range. As mentioned in section 4.1, in the intermediate depth, the mismatch between the the bound and free second harmonic wave numbers, $2K_1 - K_2$, becomes large. The solution form proposed in (4.11) with the assumption (4.13) for the second harmonic is invalid. In this situation, we must separate the bound second harmonic from the free second harmonic and rewrite

$$\phi_2(x,y) = \Psi_{2f}(x,y)e^{i\int K_2(\epsilon x)dx} + \Psi_{2b}(x,y)e^{i\int 2K_1(\epsilon x)dx} \tag{5.6}$$

to replace (4.11) for $n = 2$, where Ψ_{2f} and Ψ_{2b} are the slowly varying amplitude functions of the free and bound second harmonic, respectively. After applying the parabolic approximation, Ψ_{2f} satisfies the homogeneous equation (4.17) ($n = 2$) while Ψ_{2b} is a particular solution to (4.17) ($n = 2$) with K_2 being replaced by $2K_1$. Because the energy transfer between the first and second harmonic primarily depends on the magnitude of the phase mismatch (Madsen &

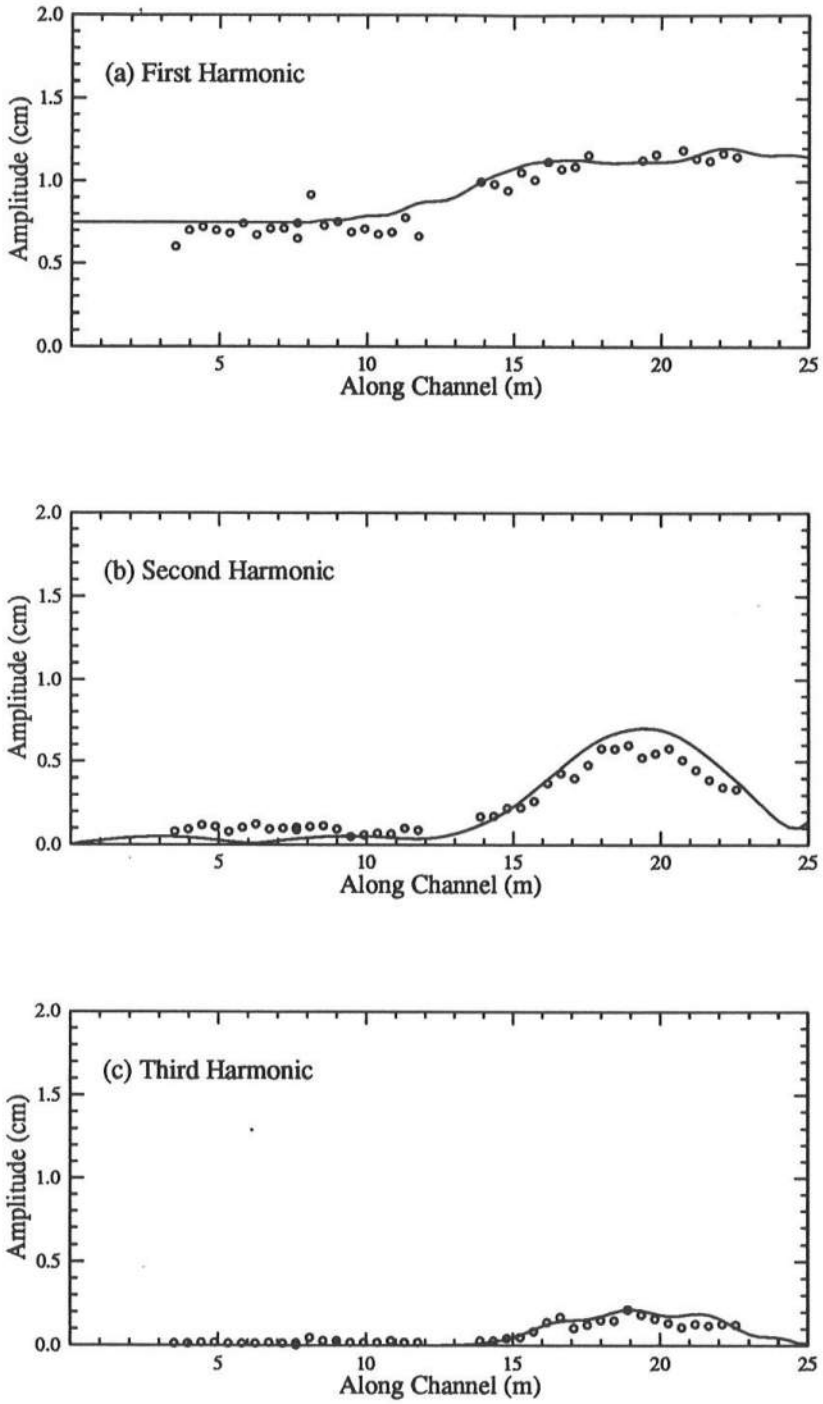

Figure 6: Wave amplitude along the centerline of the wave tank for $T = 2.0s$ and $a_0 = 0.75cm$: —— numerical results (small-angle model); o o o experimental data (Whalin, 1971).

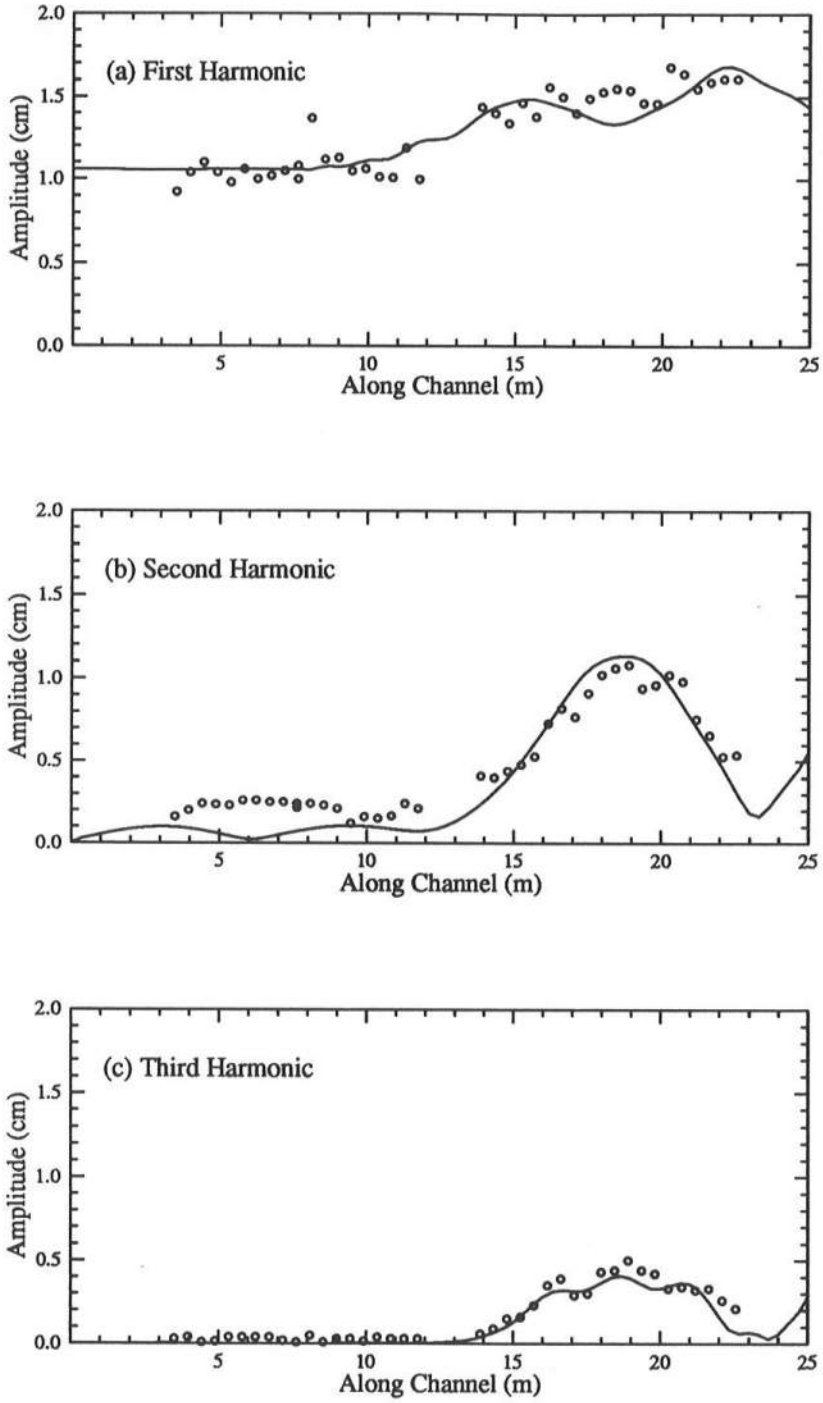

Figure 7: Wave amplitude along the centerline of the wave tank for $T = 2.0s$ and $a_0 = 1.06cm$: —— numerical results (small-angle model); o o o experimental data (Whalin, 1971).

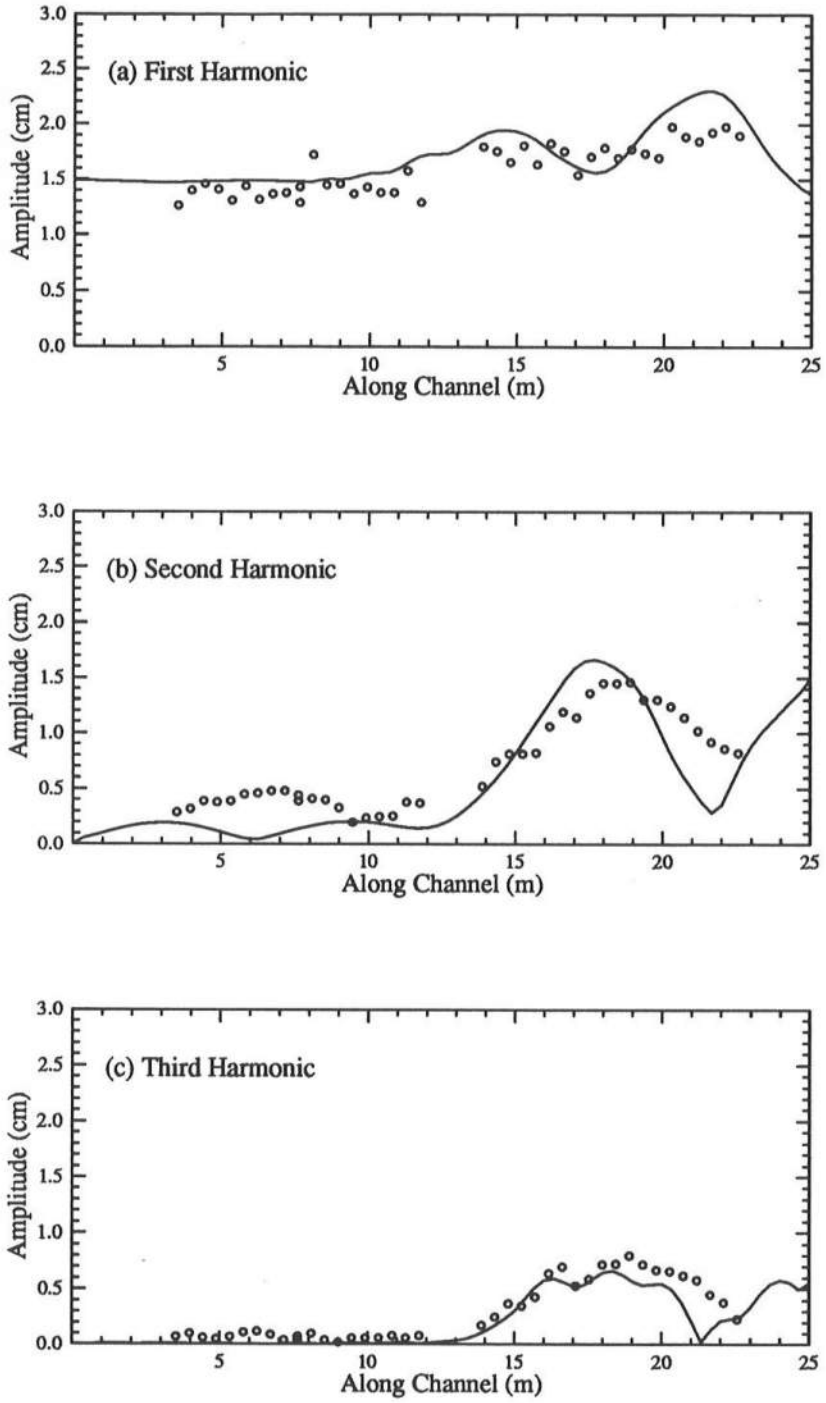

Figure 8: Wave amplitude along the centerline of the wave tank for $T = 2.0s$ and $a_0 = 1.49cm$: —— numerical results (small-angle model); o o o experimental data (Whalin, 1971).

Sorensen, 1993), for long waves, $K_2 \approx 2K_1$, the the amplitude of the second harmonic is in the same order of magnitude as that of the first harmonic (so called near-resonant phenomenon). However, for intermediate or short waves, the magnitude of the phase mismatch is of the magnitude of one and the amplitude of the second harmonic is one order smaller than that of the first harmonic. Thus, we can expect that the order of magnitude of Ψ_{2f} and Ψ_{2b} to be $O(\varepsilon)$. Therefore, in the governing equation for Ψ_{2b}, all the terms involving derivatives are $O(\varepsilon^2)$ and Ψ_{2b} can be approximated as

$$\Psi_{2b} = -i\omega\varepsilon\sigma_{21}\Psi_1^2/(2P_2) \tag{5.7}$$

where

$$P_2 = -\beta_2(2K_1)^2 + 4\omega^2 + (\alpha + 1/3)\mu^2 h^3(2K_1)^4$$

and σ_{21} is given by (4.21) with K_2 being replaced by $2K_1$. The amplitude function for the free second order harmonic, Ψ_{2f}, can be obtained by solving the homogeneous equation (4.17) ($n = 2$) with an appropriate boundary condition. However, it should be stressed that the modified Boussinesq equations and the associated parabolic equations are derived for the relative depth within the range [0, 0.5]. If accurate free second harmonic is needed, the relative depth for the free second harmonic h_0/λ_2 should be within this range. For the cases of $T = 1.0s$ (see table 1), although $h_0/\lambda_1 = 0.2913$ is within the range [0, 0.5], $h_0/\lambda_2 = 1.1175$ is far beyond this range. When the optimal value $\alpha = -0.3855$ is used, the maximum relative errors of phase and group velocities over [0, 1.1725] are 18.12% and 73.02%, respectively. Thus, the modified Boussinesq equations and their associated parabolic equations are unable to describe the free second harmonic accurately for cases of $T = 1.0s$ in Whalin's experiments. In following numerical computations, we neglect the free second harmonic.

Figures 9 and 10 show the comparison of the model results with experimental data for $T = 1.0s, a_0 = 0.97cm$ and $a_0 = 1.95cm$ ($N = 2, \Delta x = 0.1m$), respectively. Only bound second harmonic are considered. Figure 9 shows that the agreement between numerical results and experimental data is good. This indicates that the free second harmonic indeed can

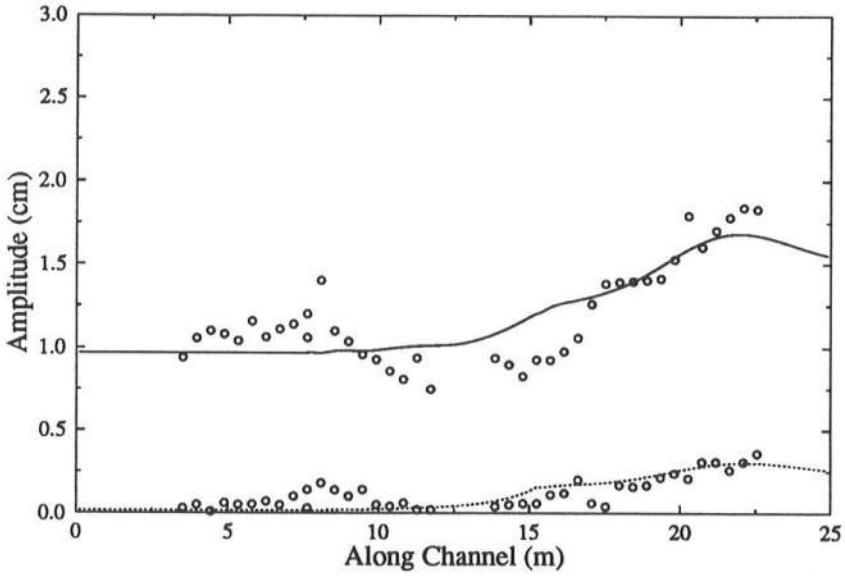

Figure 9: Wave amplitude along the centerline of the wave tank for $T = 1.0s$ and $a_0 = 0.97cm$ without the free second harmonic: —— model result for the first harmonic; $\cdots$ model result for the second harmonic; o o o experimental data (Whalin, 1971).

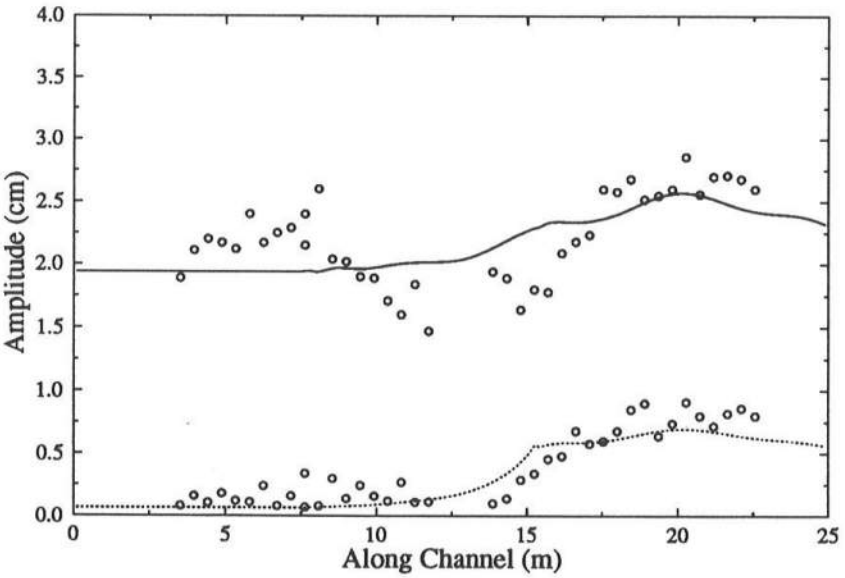

Figure 10: Wave amplitude along the centerline of the wave tank for $T = 1.0s$ and $a_0 = 1.95cm$ without the free second harmonic: —— model result for the first harmonic; $\cdots$ model result for the second harmonic; o o o experimental data (Whalin, 1971).

be neglected for $a_0 = 0.97cm$ case. However, if the nonlinearity increases, the free second harmonic may become as important as the bound second harmonic. As shown in figure 10, the underestimation of numerical results for $a_0 = 1.95cm$ in the focal region indicates that in this case the free second harmonic can not be neglected. The coexistence of the free and bound second harmonic for $a_0 = 1.95cm$ case will cause the amplitude to oscillate as observed in the experiment because each one propagates with a quite different speed. This oscillation phenomenon was not shown in Nwogu's numerical results (Nwogu, 1993b). Although Madsen & Sorensen showed this oscillation phenomenon, the accuracy of their numerical results for this case is doubtful because their new form of Boussinesq equations, which have the same linearized dispersion relation as the modified Boussinesq equations do, can not simulate the propagation of the free second harmonic accurately for $T = 1.0s$ cases in Whalin's experiments either.

5.2 Wide-angle parabolic model

The wide-angle model is applied to study the refraction of a cnoidal wave and the oblique interactions of two identical cnoidal wavetrains in a constant depth.

To construct a cnoidal wavetrain, infinite number of harmonics should be used. In actual numerical integration, we can, however, only include a finite number of harmonics. Yoon & Liu (1989) have demonstrated that a degree of unsteadiness exists when the first several harmonics in Fourier series of the cnoidal wave solution to the KdV equation are retained as an input to their parabolic model. This is true for any parabolic model. Therefore, to study cnoidal waves with the wide-angle model, we must choose appropriate initial conditions for the numerical integration that lead to permanent cnoidal wave forms in the constant depth region.

Kirby's (1991) approach is adopted here to obtain a uniform cnoidal wave that comprise only finite harmonics in a constant depth. We expand the velocity potential Φ_α and the free

surface displacement ζ in finite series

$$\Phi_a(x,t) = \sum_{n=1}^{N} \varphi_n \sin[n(kx - \omega t)], \qquad \zeta(x,t) = \sum_{n=1}^{N} a_n \cos[n(kx - \omega t)] \tag{5.8}$$

which represent a permanent cnoidal wave with φ_n, a_n and k to be determined. A set of nonlinear algebraic equations for φ_n, a_n and k can be derived from the parabolic equation, (4.23), the corresponding dimensional expression for the free surface displacement, (4.24), and the relation between the wave height of a uniform cnoidal wave and the amplitude of each harmonic. Newton-Raphson method is used to obtain φ_n, a_n and k for given wave period T, wave height H and water depth h. Details are given in appendix C.

The initial conditions of a uniform cnoidal wave with an angle of incidence θ_0 for the wide-angle model are given as

$$\phi_n(0,y) = -i\varphi_n e^{inky\sin\theta_0}, \qquad \eta_n^l(0) = \sum_{m=0}^{2M-1} Q_{ml}\phi_n^m(0) \tag{5.9}$$

When $\theta_0 \neq 0$, the periodicity condition in the y-direction requires

$$L = \frac{2\pi}{k\sin\theta_0} p \tag{5.10}$$

where $p(\neq 0)$ is an arbitrary integer.

Figure 11 shows the contour lines of $\zeta(x,y,0) = 0$ for a uniform cnoidal wave with an angle of incidence $\theta_0 = 60°$. The corresponding wave parameters are $T = 3.0s, h = 0.6317m$ and $H = 0.0522m$. Seven harmonics ($N = 7$) are considered. The wide-angle model maintains the uniformity of the incident wave as the wave propagates toward the shoreline. To obtain more quantitative details, we plot the free surface elevation and velocity potential along the straight line perpendicular to the wave crests (the dashed line in figure 11) as well as the analytical results from expressions (5.8). They agree very well as shown in figure 12. For comparison, the exact free surface elevation obtained directly from the cnoidal wave solution to the KdV equation is also plotted in figure 12 (dashed line). The wavelength given by the cnoidal wave

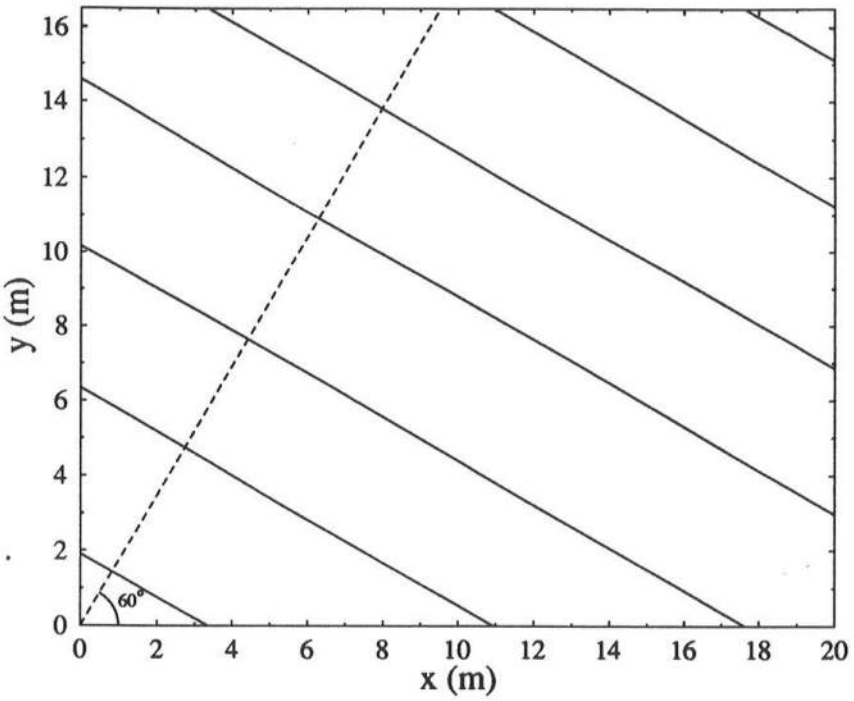

Figure 11: Contour lines of $\zeta(x, y, 0) = 0$ for a cnoidal wave with angle of incidence $\theta_0 = 60^o$.

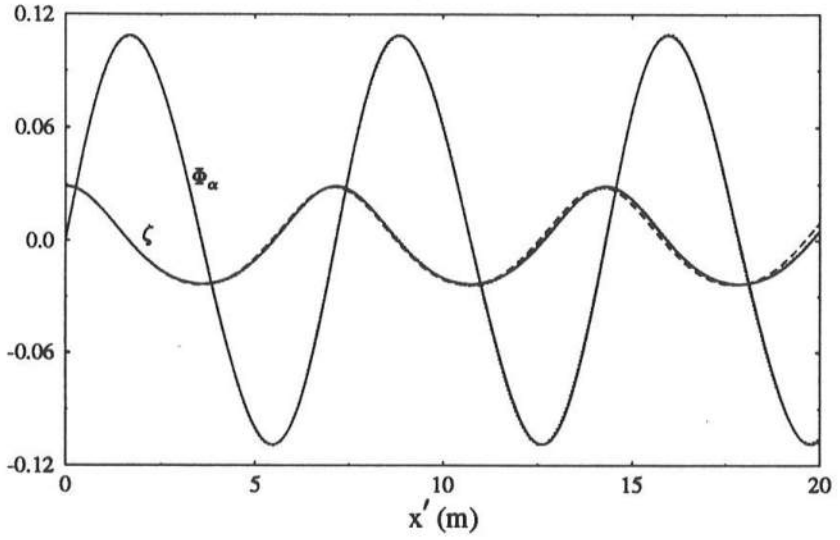

Figure 12: The comparison among the results obtained from the wide-angle model (——), the expressions (5.8) (· · · ·) and the cnoidal wave solution to the KdV equation (- - - -).

theory is $L = 2\pi/k = 7.087m$ while the wavelength obtained by Newton-Raphson technique is $L = 2\pi/k = 7.146m$. The relative error is within 1%.

Skovgaard and Petersen (1977) developed a theoretical solution for the depth refraction of first-order cnoidal waves for a quasi two-dimensional situation, i.e. for a gently sloping bathymetry whose contour lines are straight and parallel to the shoreline. With the basic assumption that the energy flux is constant between adjacent wave orthogonals, they derived two nonlinear algebraic equations for the wave height and the elliptic parameter.

To compare our wide-angle model with the cnoidal wave refraction theory, we have chosen the top row in table 1 in Skovgaard and Petersen's (1977) paper as the incident wave parameters:

$$\frac{h_0}{L_0} = 0.045, \qquad \frac{H_0}{h_0} = 0.0826, \qquad \theta_0 = 25.9^o \tag{5.11}$$

where H_0 and h_0 are the wave height and water depth at $x = 0$, respectively, and $L_0 = gT^2/2\pi$ is the deep water wave length. For incoming cnoidal wave with period $T = 3.0s$, the following parameters are used: $L_0 = 14.04m$, $h_0 = 0.6317m$ and $H_0 = 0.0522m$. The topography is given as

$$h(x) = 0.6317 - 0.03x \ (m) \tag{5.12}$$

$N = 7$ and $M = 16$ are used and the numerical integration is carried out from $x = 0$ to $x = 17m$ with marching step $\Delta x = 0.1m$. The computational domain in the y-direction is $L = 16.35m$ ($p = 1$ in (5.10)). The comparison of numerical results with theoretical results is shown in figure 13. The agreement is very satisfactory when $H/h \leq 0.4$, i.e. the nonlinearity is not too strong. When the beach slope, 0.03 (in the expression (5.12)), is replaced by a gentler slope, 0.025, numerical results do not change. This is consistent with the assumption of the cnoidal wave refraction theory that the wave height is independent of the slope of the topography (as long as it is very mild). For the same wave condition, figure 14 shows the dimensionless wave height H/h as a function of the dimensionless water depths h/L_0 for different angles of incidence: $\theta_0 = 0^o$, $\theta_0 = 30^o$ and $\theta_0 = 45^o$. The wave height decreases as the angle of incidence increases.

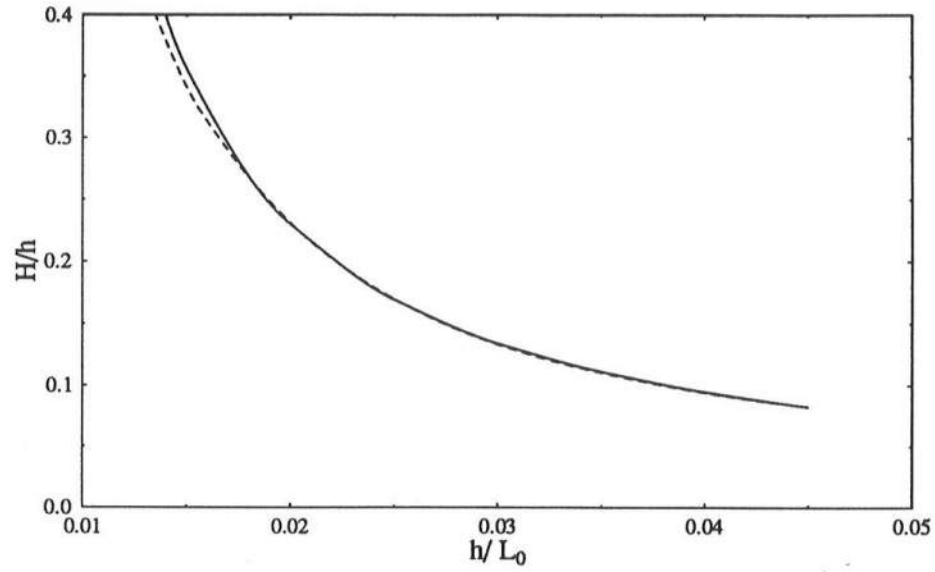

Figure 13: Refraction of a cnoidal wave over a mild-slope plain beach. ——— , cnoidal wave refraction theory results (Skovgaard and Petersen, 1977); - - - - , wide-angle model results.

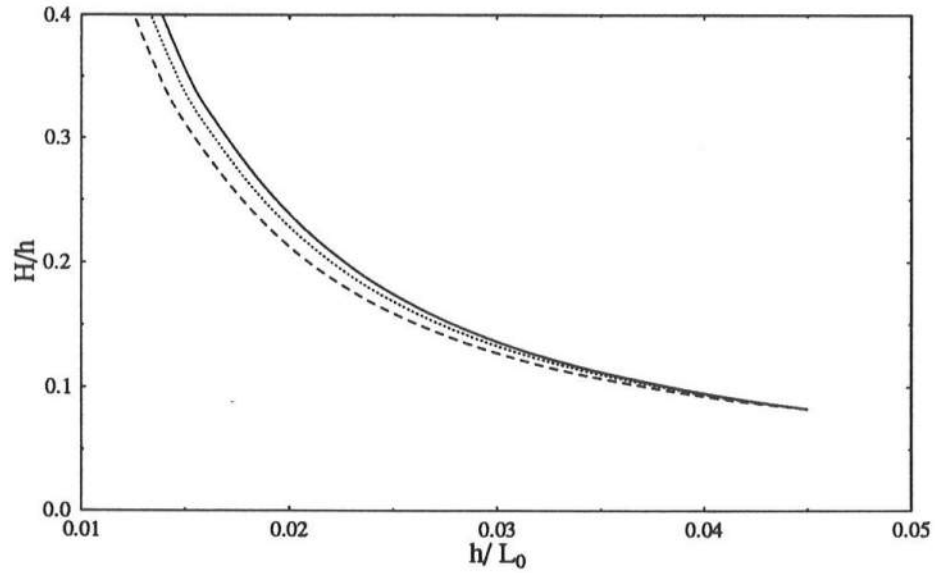

Figure 14: Dimensionless wave height H/h as a function of dimensionless water depth h/L_0 for different angles of incidence: ——— , $\theta_0 = 0^o$; $\cdots\cdots$, $\theta_0 = 30^o$; - - - , $\theta_0 = 45^o$.

Comparing the genus 2 solution to the K-P equation with the solution based on the linear superposition of two cnoidal waves, Hammack et al. (1989) showed the importance of nonlinear interactions between two identical cnoidal waves over a constant depth with directed wave angles $\pm\theta_0$. The K-P equation can only correctly describe the long wave propagation with modest transverse modulation. If the directed wave angle is large, e.g. $\theta_0 \geq 30^o$, the K-P equation becomes inadequate for modelling wave propagation. In this situation, one may use the wide-angle model instead.

Now we apply the wide-angle model to study the influence of the directed wave angle $\pm\theta_0$ on the oblique interaction of two identical cnoidal waves. The wave parameters used in our computations are very close to those of Hammack et al.'s experiment (KP1515 in table 1 in their paper): $T = 2.55s$, $h = 0.3m$ and $H = 0.02m$. Two different directed angles are considered: $\theta_0 = 22.5^o$ and $\theta_0 = 45^o$, which represent small and large directed wave angles respectively. $N = 5$, $M = 25$ and $p = 2$ are used in numerical computations. The domain of computation covers two spatial periods. Figures 15 and 16 show the comparison of the contour plots of the free surface displacement for the nonlinear interaction and linear superposition of two cnoidal waves with directed angles $\theta_0 = \pm 45^o$ and $\theta_0 = \pm 22.5^o$ respectively. The values of contour lines are from $-1.5cm$ to $2.0cm$ with an increment $0.5cm$. In figure 15, for large directed wave angles, the difference between the nonlinear solutions and solutions from the linear superposition is very small. On the other hand, for a smaller directed wave angle, figure 16 shows that the difference is quite large and nonlinear numerical solutions evolve along the x-direction. From the perspective pictures shown in figures 17 and 18, we observe that the nonlinear interaction increases the length of a crest. This was also observed in laboratory experiments (Hammack et al., 1989).

6 Concluding Remarks

We formally derive the modified Boussinesq equations in terms of the velocity potential, $\Phi_\alpha(x, y, t)$, evaluated on an arbitrary elevation $z = z_\alpha(x, y)$, and the free surface displace-

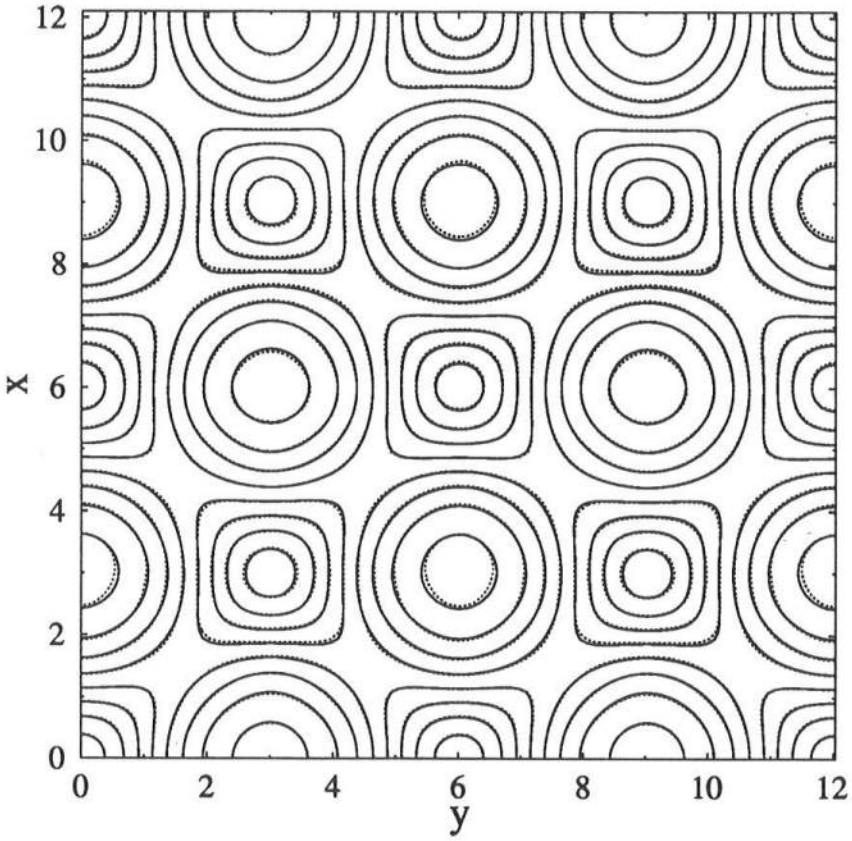

Figure 15: The comparison of contour plots of $\zeta(x, y, 0)$ for linear superposition and nonlinear interaction of two cnoidal waves with directed wave angles $\theta_0 = \pm 45°$: ——, linear superposition; $\cdots\cdot$, nonlinear interaction.

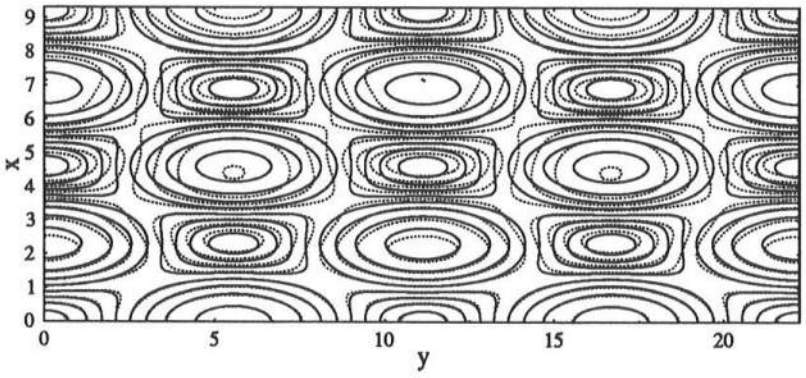

Figure 16: The comparison of contour plots of $\zeta(x, y, 0)$ for linear superposition and nonlinear interaction of two identical cnoidal waves with directed wave angles $\theta_0 = \pm 22.5°$: —— , linear superposition; $\cdots\cdot$, nonlinear interaction.

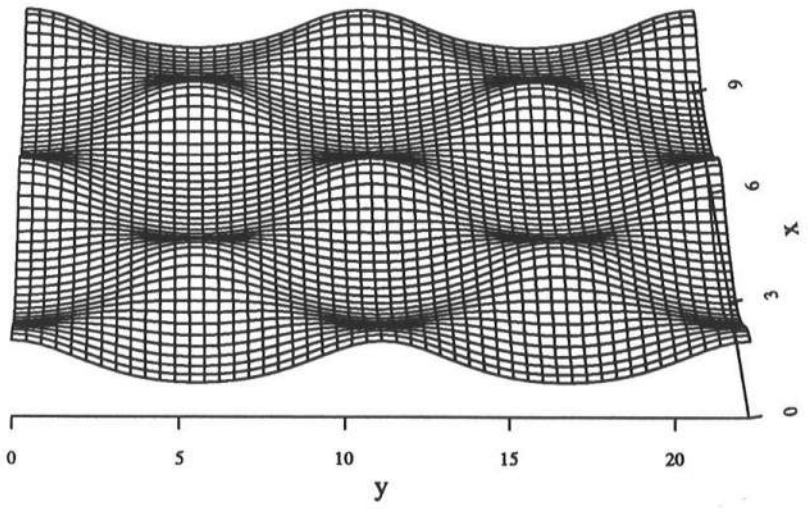

Figure 17: A perspective view of free surface elevations of nonlinear interaction of two identical cnoidal wavetrains with directed wave angles $\theta_0 = \pm 22.5^o$.

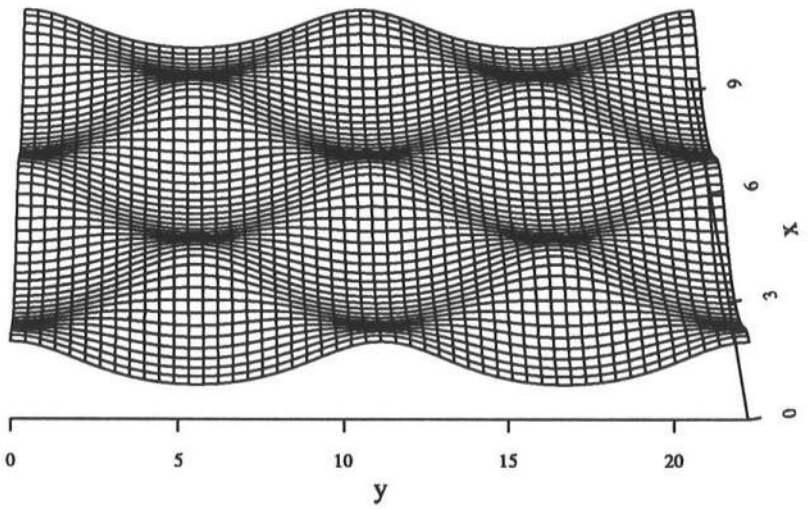

Figure 18: A perspective view of free surface elevations of linear superposition of two identical cnoidal wavetrains with directed wave angles $\theta_0 = \pm 22.5^o$.

ment. We show that when $\Phi_\alpha(x,y)$ is evaluated at $z=-0.522h$, the corresponding modified Boussinesq equations have almost the same dispersive behavior as that for the first-order Stokes wave for water depths ranging from $h/\lambda_0 = 0$ to 0.5, where λ_0 represents the wavelength in deep water.

Both small-angle parabolic model, (4.17), and wide-angle parabolic model, (4.49), for regular waves are derived. They can also be applied to simulate irregular wave propagation by discretizing the power spectrum of the incident wave evenly (Freilich & Guza, 1984). The wide-angle model is restricted to the situations where the deviation of the actual topography from a reference water depth (which varies in the on-offshore only) is in the same order of magnitude as the typical wave amplitude.

Although we have shown in many examples that the modified Boussinesq equations can be extended to simulate wave propagation from deep water to shallow water, the velocity field calculated from (2.11) does not give accurate results in deep water. When the velocity field is essential, we suggest an empirical formula to calculate the vertical variation of the velocity potential water once the velocity potential $\Phi_\alpha(x,y,t)$ is found.

$$\Phi(x,y,z,t) = \frac{\cosh k(z+h)}{\cosh k(z_\alpha+h)}\Phi_\alpha(x,y,t) \tag{6.1}$$

For an infinitesimal amplitude, periodic wave propagating in the x-direction over a constant depth, the maximum relative errors between the velocity components (u,w) given by above empirical formula and exact velocity components (u_L,w_L) (without considering the nonlinearity) given by the Stokes first-order theory over the range $h/\lambda_0 \in [0,0.5]$ and $z/h \in [-1,0]$ are

$$\max_{h/\lambda_0\in[0,0.5],z/h\in[-1,0]}\left[\frac{|u|}{|u_L|}-1\right] = 2.93\% \tag{6.2}$$

$$\max_{h/\lambda_0\in[0,0.5],z/h\in[-1,0]}\left[\frac{|w|}{|w_L|}-1\right] = 2.94\% \tag{6.3}$$

In deep water, the nonlinearity should be very small to ensure the weakly nonlinearity assumption is still valid in the shallow region. Therefore, as long as the the bottom variation is

small, the empirical formula (6.1) is a plausible way to find the velocity field in deep water.

Acknowledgement

This research has been supported by a research grant from New York Sea Grant Institute and a research grant from the Army Research Office (DAAL 03-92-G-0116).

Appendix A

This appendix gives the corresponding dimensional forms of the expressions mentioned in sections 4.1 and 4.2. All variables shown in this appendix are dimensional, however, primes have been dropped for simplicity.

The dimensional quantities appeared in (4.23) can be given as:

$$\beta_n = h + \alpha \frac{n^2\omega^2}{g} h^2 \tag{A.1}$$

$$\tau_n = 1 + z_\alpha \frac{n^2\omega^2}{g} \tag{A.2}$$

$$W_n = \beta_n - 2(\alpha + 1/3)h^3 K_n^2 \tag{A.3}$$

$$R_n = \tau_n - C_\alpha h^2 K_n^2 \tag{A.4}$$

$$K_n^2 = \frac{g + \alpha n^2\omega^2 H - \sqrt{(g + \alpha n^2\omega^2 H)^2 - 4(\alpha + 1/3)g n^2\omega^2 H}}{2(\alpha + 1/3)gH^2} \tag{A.5}$$

$$P_n = -\beta_n K_n^2 + \frac{n^2\omega^2}{g} + (\alpha + 1/3)h^3 K_n^4 + i\left[\beta_n - 6(\alpha + 1/3)h^3 K_n^2\right] \frac{dK_n}{dx} \tag{A.6}$$

$$\sigma_{ns} = sK_{n-s} e^{i\int (K_s + K_{n-s} - K_n)dx} \left[\alpha h^2 K_s^2 (K_s + K_{n-s}) - (2K_s + K_{n-s})\right] \tag{A.7}$$

$$\begin{aligned} \gamma_{ns} = e^{i\int (K_{n+s} - K_s - K_n)dx} \Big[& nK_s K_{n+s}(2 + \alpha h^2 K_s K_{n+s}) \\ & + sK_{n+s}(K_{n+s} + \alpha h^2 K_s^3) - (n+s)K_s(K_s + \alpha h^2 K_{n+s}^3)\Big] \end{aligned} \tag{A.8}$$

The corresponding dimensional expression for the free surface displacement, (4.24), is given as

$$g\zeta_n e^{-i\int K_n dx} = in\omega\Psi_n + in\omega\left\{\alpha h^2\left[\left(i\frac{dK_n}{dx} - K_n^2\right)\Psi_n + 2iK_n\frac{\partial\Psi_n}{\partial x} + \frac{\partial^2\Psi_n}{\partial y^2}\right]\right.$$
$$\left. + z_\alpha\left(iK_n\Psi_n\frac{\partial h}{\partial x} + \frac{\partial h}{\partial y}\frac{\partial\Psi_n}{\partial y}\right)\right\} + \frac{1}{4}\left[\sum_{s=1}^{n-1} K_s K_{n-s}\Psi_s\Psi_{n-s}e^{i\int(K_s+K_{n-s}-K_n)dx}\right.$$
$$\left. - 2\sum_{s=1}^{N-n} K_s K_{n+s}\overline{\Psi}_s\Psi_{n+s}e^{i\int(K_{n+s}-K_s-K_n)dx}\right] \tag{A.9}$$

The dimensional expressions for B_n, D_n, E_{nl}, U_n^m and V_n^m appeared in the wide-angle model (4.52) are given as follows:

$$B_n = H + \alpha\frac{n^2\omega^2}{g}H^2 \tag{A.10}$$

$$D_n = B_n - 2(\alpha + 1/3)H^3K_n^2 \tag{A.11}$$

$$E_{nl} = B_n - 2(\alpha + 1/3)H^3(3K_n^2 - 2\lambda_l^2) \tag{A.12}$$

$$U_n^m = (\beta_n^m - B_n)\left[\frac{d^2\phi_n^m}{dx^2} + \Lambda_0\frac{\partial^2\phi_n^m}{\partial\tilde{y}^2}\right] + (\alpha + 1/3)[(h^m)^3 - H^3]\left[\frac{d^4\phi_n^m}{dx^4} + \right.$$
$$\left. 2\Lambda_0\frac{\partial^4\phi_n^m}{\partial x^2\partial\tilde{y}^2} + \Lambda_0^2\frac{\partial^4\phi_n^m}{\partial\tilde{y}^4}\right] + \tau_n^m\left[\frac{dh^m}{dx}\frac{d\phi_n^m}{dx} + \Lambda_0\frac{\partial h^m}{\partial\tilde{y}}\frac{\partial\phi_n^m}{\partial\tilde{y}}\right] + (h^m)^2C_\alpha$$
$$\left[\frac{dh^m}{dx}\left(\frac{d^3\phi_n^m}{dx^3} + \Lambda_0\frac{\partial^3\phi_n^m}{\partial x\partial\tilde{y}^2}\right) + \Lambda_0\frac{\partial h^m}{\partial\tilde{y}}\left(\frac{\partial^3\phi_n^m}{\partial x^2\partial\tilde{y}} + \Lambda_0\frac{\partial^3\phi_n^m}{\partial\tilde{y}^3}\right)\right] \tag{A.13}$$

$$V_n^m = \sum_{s=1}^{n-1} s\left\{2\left[\frac{d\phi_s^m}{dx}\frac{d\phi_{n-s}^m}{dx} + \Lambda_0\frac{\partial\phi_s^m}{\partial\tilde{y}}\frac{\partial\phi_{n-s}^m}{\partial\tilde{y}}\right] + \alpha(h^m)^2\left[\left(\frac{d^3\phi_s^m}{dx^3} + \Lambda_0\frac{\partial^3\phi_s^m}{\partial x\partial\tilde{y}^2}\right)\right.\right.$$
$$\left.\frac{d\phi_{n-s}^m}{dx} + \Lambda_0\left(\frac{\partial^3\phi_s^m}{\partial x^2\partial\tilde{y}} + \Lambda_0\frac{\partial^3\phi_s^m}{\partial\tilde{y}^3}\right)\frac{\partial\phi_{n-s}^m}{\partial\tilde{y}}\right] + \left[\phi_s^m + \alpha(h^m)^2\left(\frac{d^2\phi_s^m}{dx^2} + \right.\right.$$
$$\left.\left.\left.\Lambda_0\frac{\partial^2\phi_s^m}{\partial\tilde{y}^2}\right)\right]\left[\frac{d^2\phi_{n-s}^m}{dx^2} + \Lambda_0\frac{\partial^2\phi_{n-s}^m}{\partial\tilde{y}^2}\right]\right\} + \sum_{s=1}^{N-n}\left\{n\left[2\left(\frac{d\bar{\phi}_s^m}{dx}\frac{d\phi_{n+s}^m}{dx} + \right.\right.\right.$$
$$\left.\left.\Lambda_0\frac{\partial\bar{\phi}_s^m}{\partial\tilde{y}}\frac{\partial\phi_{n+s}^m}{\partial\tilde{y}}\right) + \alpha(h^m)^2\left(\frac{d^2\bar{\phi}_s^m}{dx^2} + \Lambda_0\frac{\partial^2\bar{\phi}_s^m}{\partial\tilde{y}^2}\right)\left(\frac{d^2\phi_{n+s}^m}{dx^2} + \Lambda_0\frac{\partial^2\phi_{n+s}^m}{\partial\tilde{y}^2}\right)\right] -$$

$$s\left[\alpha(h^m)^2[(\frac{d^3\bar{\phi}_s^m}{dx^3}+\Lambda_0\frac{\partial^3\bar{\phi}_s^m}{\partial x\partial\tilde{y}^2})\frac{d\phi_{n+s}^m}{dx}+\Lambda_0(\frac{\partial^3\bar{\phi}_s^m}{\partial x^2\partial\tilde{y}}+\Lambda_0\frac{\partial^3\bar{\phi}_s^m}{\partial\tilde{y}^3})\frac{\partial\phi_{n+s}^m}{\partial\tilde{y}}]+\right.$$
$$\left.\bar{\phi}_s^m(\frac{d^2\phi_{n+s}^m}{dx^2}+\Lambda_0\frac{\partial^2\phi_{n+s}^m}{\partial\tilde{y}^2})\right]+(n+s)\left[\alpha(h^m)^2[(\frac{d^3\phi_{n+s}^m}{dx^3}+\Lambda_0\frac{\partial^3\phi_{n+s}^m}{\partial x\partial\tilde{y}^2})\frac{d\bar{\phi}_s^m}{dx}+\right.$$
$$\left.\left.\Lambda_0(\frac{\partial^3\phi_{n+s}^m}{\partial x^2\partial\tilde{y}}+\Lambda_0\frac{\partial^3\phi_{n+s}^m}{\partial\tilde{y}^3})\frac{\partial\bar{\phi}_s^m}{\partial\tilde{y}}]+\phi_{n+s}^m(\frac{d^2\bar{\phi}_s^m}{dx^2}+\Lambda_0\frac{\partial^2\bar{\phi}_s^m}{\partial\tilde{y}^2})\right]\right\} \tag{A.14}$$

where

$$\frac{\partial h^m}{\partial\tilde{y}}=\sum_{j=0}^{2M-1}[D_1]_{mj}h^j; \qquad \frac{\partial^3\phi_m^j}{\partial x^2\partial\tilde{y}}=\sum_{j=0}^{2M-1}[D_1]_{mj}\frac{d^2\phi_s^j}{dx^2};$$

$$\frac{\partial^3\phi_s^m}{\partial x\partial\tilde{y}^2}=\sum_{j=0}^{2M-1}[D_2]_{mj}\frac{d\phi_s^j}{dx}; \qquad \frac{\partial^4\phi_n^m}{\partial^2x\partial\tilde{y}^2}=\sum_{j=0}^{2M-1}[D_2]_{mj}\frac{d^2\phi_n^j}{dx^2};$$

and

$$\frac{d^p\phi_s^m}{dx^p};\ \frac{\partial^p\phi_s^m}{\partial\tilde{y}^p}=\left.\frac{\partial^p\phi_s(x,\tilde{y})}{\partial\tilde{y}^p}\right|_{\tilde{y}=\tilde{y}_m} \qquad (p=1,2,3,4)$$

are given by (4.45)–(4.48) and (4.33) (since the dimensional forms for (4.45)–(4.48) and (4.33) do not change).

Appendix B

In this appendix, we apply the pseudospectral Chebyshev method to solve the small-angle model for wave propagation within a channel bounded by two parallel vertical walls.

Assume the computational domain in the y-direction is $[0, L]$, the following transformation

$$y=(\tilde{y}+1)L/2 \tag{B.1}$$

maps the interval $y\in[0,L]$ into $\tilde{y}\in[-1,1]$, which is the standard interval adopted by the pseudospectral Chebyshev method. Under the above mapping, equation (4.23) becomes

$$\frac{\partial\Psi_n}{\partial x}=\frac{i}{2K_n}\left\{\Lambda\frac{\partial^2\Psi_n}{\partial\tilde{y}^2}+\frac{1}{W_n}\left[\left(P_n+iR_nK_n\frac{\partial h}{\partial x}\right)\Psi_n+\Lambda R_n\frac{\partial h}{\partial\tilde{y}}\frac{\partial\Psi_n}{\partial\tilde{y}}\right.\right.$$

$$+\frac{i\omega}{2g}\left(\sum_{s=1}^{n-1}\sigma_{ns}\Psi_s\Psi_{n-s}+\sum_{s=1}^{N-n}\gamma_{ns}\overline{\Psi}_s\Psi_{n+s}\right)\Bigg]\Bigg\} \tag{B.2}$$

where

$$\Lambda=(2/L)^2$$

Now we approximate $\Psi_n(x,\tilde{y})$ in $\tilde{y}$-direction by a M-th degree polynomial at the following Chebyshev extreme points (Gottlieb et al. 1984):

$$\tilde{y}_j=\cos\frac{\pi j}{M}\quad(0\le j\le M) \tag{B.3}$$

$$\Psi_n(x,\tilde{y})=\sum_{j=0}^{M}g_j(\tilde{y})\Psi_n^j(x) \tag{B.4}$$

where $\Psi_n^j(x)=\Psi_n(x,\tilde{y}_j)$ and the interpolant $g_j(\tilde{y})$ is defined as

$$g_j(\tilde{y})=\frac{(1-\tilde{y}^2)(-1)^{j+1}}{\bar{c}_jM^2(\tilde{y}-\tilde{y}_j)}\frac{dT_M(\tilde{y})}{d\tilde{y}} \tag{B.5}$$

with $\bar{c}_0=\bar{c}_M=2,\bar{c}_j=1\ (1\le j\le M-1)$ and $T_M(\tilde{y})=\cos(M\cos^{-1}\tilde{y})$ is the M-th order Chebyshev polynomial. It is readily verified that

$$g_j(\tilde{y}_k)=\delta_{jk} \tag{B.6}$$

The p-th order partial derivative of $\Psi_n(x,\tilde{y})$ with respect to $\tilde{y}$ evaluated at the collocation point $\tilde{y}_m$ can be expressed as the linear combination of $\Psi_n^j\ (0\le j\le M)$

$$\left.\frac{\partial^p\Psi_n(x,\tilde{y})}{\partial\tilde{y}^p}\right|_{\tilde{y}=\tilde{y}_m}=\sum_{j=0}^{M}\Psi_n^j(x)\left.\frac{d^pg_j(\tilde{y})}{d\tilde{y}^p}\right|_{\tilde{y}=\tilde{y}_m}=\sum_{j=0}^{M}[D_p]_{mj}\Psi_n^j(x) \tag{B.7}$$

where

$$[D_p]_{mj}=\left.\frac{d^pg_j(\tilde{y})}{d\tilde{y}^p}\right|_{\tilde{y}=\tilde{y}_m} \tag{B.8}$$

which is a $(M+1)\times(M+1)$ matrix and has an analytical expression:

$$D_p = (D_1)^p \tag{B.9}$$

and

$$[D_1]_{mj} = \frac{\bar{c}_m(-1)^{m+j}}{\bar{c}_j(\tilde{y}_m - \tilde{y}_j)} \quad (m \neq j) \tag{B.10}$$

$$[D_1]_{jj} = -\frac{\tilde{y}_j}{2(1-\tilde{y}_j^2)}; \quad [D_1]_{00} = \frac{2M^2+1}{6} = -[D_1]_{MM} \tag{B.11}$$

It should be noted from the above explicit formulas that the matrix D_1 is not anti-symmetric and D_2 is not symmetric. These features prevent us from extending the pseudospectral Chebyshev method to develop a corresponding wide-angle parabolic model. Fortunately, for waves propagating in a straight channel the small-angle approximation is adequate.

Substituting (B.4) into (B.2) and evaluating the resulting equation at $\tilde{y} = \tilde{y}_m$ $(1 \leq m \leq M-1)$, noting (B.6) and (B.7), we have

$$\begin{aligned}\frac{d\Psi_n^m}{dx} = \frac{i}{2K_n}\Bigg\{\Lambda\sum_{j=0}^{M}[D_2]_{mj}\Psi_n^j + \frac{1}{W_n^m}\Bigg[\left(P_n^m + iR_n^m K_n\frac{dh^m}{dx}\right)\Psi_n^m \\ + \Lambda R_n^m\sum_{j=0}^{M}[D_1]_{mj}h^j\sum_{j=0}^{M}[D_1]_{mj}\Psi_n^j + \frac{i\omega}{2g}\Bigg(\sum_{s=1}^{n-1}\sigma_{ns}^m\Psi_s^m\Psi_{n-s}^m \\ + \sum_{s=1}^{N-n}\gamma_{ns}^m\overline{\Psi}_s^m\Psi_{n+s}^m\Bigg)\Bigg]\Bigg\} \qquad (1\leq m\leq M-1)\end{aligned} \tag{B.12}$$

where the superscript m indicates that the corresponding variable is evaluated at $\tilde{y} = \tilde{y}_m$ and

$$h(x,\tilde{y}) = \sum_{j=0}^{M} g_j(\tilde{y})h^j(x) \tag{B.13}$$

For each harmonic (B.12) provides $(M-1)$ ordinary differential equations for $(M+1)$ unknowns Ψ_n^m $(0 \leq m \leq M)$, the other two equations are provided by the no-flux boundary conditions

$$\frac{\partial\Psi_n}{\partial\tilde{y}} = 0; \text{ at } \tilde{y} = \pm 1 \tag{B.14}$$

Replacing the differentiation operator by the differentiation matrix in (B.14), we have

$$\sum_{j=0}^{M}[D_1]_{0j}\Psi_n^j = 0; \quad \sum_{j=0}^{M}[D_1]_{Mj}\Psi_n^j = 0 \tag{B.15}$$

Since

$$\det = [D_1]_{00}[D_1]_{MM} - [D_1]_{0M}[D_1]_{M0} = -\left(\frac{2M^2+1}{6}\right)^2 + \frac{1}{4} \neq 0 \tag{B.16}$$

Ψ_n^0 and Ψ_n^M can be expressed in terms of $\Psi_n^j (1 \leq j \leq M-1)$

$$\Psi_n^0 = \frac{1}{\det}\left\{[D_1]_{0M}\sum_{j=1}^{M-1}[D_1]_{Mj}\Psi_n^j - [D_1]_{MM}\sum_{j=1}^{M-1}[D_1]_{0j}\Psi_n^j\right\} \tag{B.17}$$

$$\Psi_n^M = \frac{1}{\det}\left\{[D_1]_{M0}\sum_{j=1}^{M-1}[D_1]_{0j}\Psi_n^j - [D_1]_{00}\sum_{j=1}^{M-1}[D_1]_{Mj}\Psi_n^j\right\} \tag{B.18}$$

By solving (B.12) with boundary conditions (B.17) and (B.17), we can find $\Psi_n(x,y)$ $(n = 1,\ldots,N)$.

Appendix C

This appendix gives the detail procedure to find a uniform cnoidal wave from the small-angle model.

We rewrite (4.1) and (4.2) as

$$\Phi_\alpha = \sum_{n=1}^{N}\frac{\phi_n}{2}e^{-in\omega t} + c.c. = \sum_{n=1}^{N}-i\frac{\varphi_n}{2}e^{in(kx-\omega t)} + c.c. \tag{C.1}$$

$$\zeta = \sum_{n=1}^{N}\frac{\zeta_n}{2}e^{-in\omega t} + c.c. = \sum_{n=1}^{N}\frac{a_n}{2}e^{in(kx-\omega t)} + c.c. \tag{C.2}$$

where φ_n and a_n are real constants, k is the wave number of the uniform cnoidal wave.

From (4.11), we have

$$\Psi_n = -i\varphi_n e^{i(nk-K_n)x} \tag{C.3}$$

Hence the small-angle model (4.23) reads

$$\{2K_nW_n(nk-W_n)-P_n\}\varphi_n-\frac{\omega}{2g}\left(\sum_{s=1}^{n-1}\sigma'_{ns}\varphi_s\varphi_{n-s}-\sum_{s=1}^{N-n}\gamma'_{ns}\varphi_s\varphi_{n+s}\right)=0 \tag{C.4}$$

where

$$\sigma'_{ns}=sK_{n-s}\left[\alpha h^2K_s^2(K_s+K_{n-s})-(2K_s+K_{n-s})\right] \tag{C.5}$$

$$\begin{aligned}\gamma'_{ns}=&nK_sK_{n+s}(2+\alpha h^2K_sK_{n+s})+sK_{n+s}(K_{n+s}+\alpha h^2K_s^3)\\&-(n+s)K_s(K_s+\alpha h^2K_{n+s}^3)\end{aligned} \tag{C.6}$$

and K_n, W_n, P_n are given in appendix A.

Substituting

$$\zeta_n=a_ne^{inkx} \tag{C.7}$$

and (C.3) into the dimensional form of (4.24), i.e. (A.9), we have

$$\begin{aligned}a_n=\frac{1}{g}\Big\{&\left[1+\alpha h^2(K_n^2-2nkK_n)\right]n\omega\varphi_n\\&-\frac{1}{4}\left(\sum_{s=1}^{n-1}K_sK_{n-s}\varphi_s\varphi_{n-s}+2\sum_{s=1}^{N-n}K_sK_{n+s}\varphi_s\varphi_{n+s}\right)\Big\}\end{aligned} \tag{C.8}$$

The relation between the wave height of a uniform cnoidal wave and the wave amplitude of each harmonic can be expressed as:

$$H=a_1+a_3+a_5+\cdots \tag{C.9}$$

i.e. the sum of amplitude of all odd harmonics. For given wave period T, wave height H and water depth h, we use Newton-Raphson method to solve $(N+1)$ equations: (C.4) and (C.9) (after the substitution of (C.8)) for $(N+1)$ unknowns: $\varphi_n(n=1,\ldots,N)$ and k. Then

$$\Phi_\alpha(x,t)=\sum_{n=1}^{N}\varphi_n\sin[n(kx-\omega t)],\qquad \zeta(x,t)=\sum_{n=1}^{N}a_n\cos[n(kx-\omega t)] \tag{C.10}$$

will give a uniform cnoidal wave.

References

[1] Chen, Y. & Liu, P. L.-F. 1993 Scattering of linear and weakly nonlinear waves: Pseudospectral approaches. (Submitted for publication)

[2] Freilich, M.H. & Guza, R.T. 1984 Nonlinear effects on shoaling surface gravity waves. Phil. Trans. R. Soc. Lond. A **311**, 1-41.

[3] Gottlieb, D., Hussaini, M.Y. & Orszag, S.A. 1984 Introduction: Theory and applications of spectral methods. In Spectral Methods for Partial Differential Equations (ed. D. Gottlieb & M.Y. Hussaini), pp. 1-54. SIAM, Philadelphia.

[4] Hammack, J., Scheffner, N. & Segur, H. 1988 Two-dimensional periodic waves in shallow water. J. Fluid Mech. **209**, 567-589.

[5] Kadomstev, B.B. & Petviashvili, V.I. 1970 On the stability of solitary waves in weakly dispersing media. Sov. Phys. Dokl. **15**, 539-541.

[6] Kirby, J.T. 1991 Intercomparison of truncated series solutions for shallow water waves. J. Waterway, Port, Coastal and Ocean Engineering, ASCE, Vol. 117, No. 2, pp. 143-155.

[7] Kirby, J.T. 1990 Modelling shoaling directional wave spectra in shallow water. Proc. 22th Int. Conf. on Coastal Engrg., Vol 1, pp. 109-122.

[8] Liu, P. L.-F. & Tsay, T.K. 1984 Refraction-diffraction model for weakly nonlinear water waves. J. Fluid Mech. **141**, 265-274.

[9] Liu, P. L.-F., Yoon, S.B. & Kirby, J.T. 1985 Nonlinear refraction-diffraction of waves in shallow water. J. Fluid Mech. **153**, 185-201.

[10] Madsen, P.A. & Sorensen, O.R. 1992 A new form of the Boussinesq equations with improved linear dispersion characteristics. Part 2. A slowly-varying bathymetry. Coastal Engineering **18**, 183-204.

[11] Madsen, P.A. & Sorensen, O.R. 1993 Bound waves and triad interactions in shallow water. Ocean Engineering, Vol. 20, No 4, pp. 359-388.

[12] McCowan, A.D. 1987 The range of application of Boussinesq type numerical short wave models. Proc. XXII IAHR Congress, Lausanne, Switzerland, pp. 379-384.

[13] McCowan, A.D. & Blackman, D.R. 1989 The extension of Boussinesq type equations to modelling short waves in deep water. Proc. 9th Australasian Conference on Coastal and Ocean Engineering, Adelaid,Australia, pp.412-416.

[14] Nwogu, O. 1993a An alternative form of the Boussinesq equations for nearshore wave propagation. J. Waterway, Port, Coastal and Ocean Engineering, ASCE (to appear).

[15] Nwogu, O. 1993b Nonlinear transformation of multi-directional waves in water of variable depth. (Submited to Journal of Fluid Mechanics)

[16] Peregrine, D.H. 1967 Long waves on a beach. J. Fluid Mech. **27**, 815-827.

[17] Rygg, O. 1988 Nonlinear refraction-diffraction of surface waves in intermediate and shallow water. Coastal Engineering **12**, 191-211.

[18] Skovgaard, O. & Petersen, M.H. 1977 Refraction of cnoidal waves. Coastal Engineering **1**, 43-61.

[19] Whalin, R.W. 1971 The limit of applicability of linear wave refraction theory in a convergence zone. Res. Rep. H-71-3, U.S. Army Corps of Engrs, Waterways Expt. Station, Vicksburg, MS.

[20] Witting, J.M. 1984 A unified model for the evolution of nonlinear water waves. J. Comput. Phys. **56**, 203-236.

[21] Wu, T.Y. 1979 On tsunamis propagation—evaluation of existing models. In Tsunamis Proc. National Science Foundation Workshop (ed. Hwang, L.S. & Lee, Y.K.), pp. 110-149. Pasadena: Tetra Tech.

[22] Yoon, S.B. & Liu, P. L.-F. 1989 Stem waves along breakwater. J. Waterway, Port, Coastal and Ocean Engineering, ASCE, Vol. 115, No. 5, pp. 635-648.